Metformin increases tauroursodeoxycholic acid levels to improve insulin resistance in diet-induced obese mice

Ya Zhang [a,b,1], Yang Cheng [a,1], Jian Liu [a,1], Dan He [a], Jihui Zuo [a], Liping Yan [a], Ronald W. Thring [b], Mingjiang Wu [a], Yitian Gao [a,*], Haibin Tong [a,*]

[a] College of Life and Environmental Science, Wenzhou University, Wenzhou 325035, China;

[b] Environmental Science and Environmental Engineering, University of Northern British Columbia, Prince George, BC, Canada;

*Correspondence: tonghaibin@gmail.com (H.T.); gyt@wzu.edu.cn (Y.G.); Tel.: + 86-577-86689078

[1] These authors contributed equally to this study.

Abstract

Metformin is widely used to surmount insulin resistance (IR) and type 2 diabetes. Evidence indicates that metformin improves insulin resistance associated with gut microbiota, but the underlying mechanism remains unclear. In the present study, metformin effectively improved insulin sensitivity and alleviated liver inflammation and oxidative stress in high-fat diet (HFD)-fed mice. Metabolomics analysis showed that metformin increased tauroursodeoxycholic acid (TUDCA) levels both in intestinal content and liver by reducing the production and activity of bile salt hydrolase (BSH). We further found that TUDCA was able to antagonize with KEAP1 to prevent its binding to Nrf2 and activate Nrf2/ARE pathway, thereby reducing intracellular ROS and improving insulin signaling. Moreover, metformin increased the proportion of *Akkermanisia muciniphlia* in the HFD-fed mice, while *in vitro* growth curve test confirmed that it's TUDCA, not metformin, promoted the proliferation of *A. muciniphlia*. Subsequently, TUDCA administration could effectively ameliorate insulin resistance, activate hepatic Nrf2/ARE pathways, and increase the abundance of intestinal *A. muciniphlia* in *ob/ob* mice. These findings reveal that metformin remodels the gut microbiota, reduces oxidative stress and enhances insulin sensitivity partly due to increasing the production of TUDCA. This provides a novel mechanism by which metformin alleviates diet-induced insulin resistance and improves metabolism.

Keywords: Metformin; Gut microbiota; Insulin resistance; TUDCA; Nrf2

37 **Abbreviations**

38 T2DM, type 2 diabetes mellitus; AMPK, AMP-activated protein kinase; IR, insulin
39 resistance; BA, bile acids; ER, endoplasmic reticulum; BSH, bile salt hydrolase;
40 NASH, nonalcoholic steatohepatitis; ROS, reactive oxygen species; Nrf2, nuclear
41 factor-erythroid-2-related factor 2; KEAP1, Kelch-like ECH-associated protein 1;
42 TUDCA, tauroursodeoxycholic acid; IRS-1, insulin receptor substrate 1; Akt, protein
43 kinase B; 4-HNE, 4-hydroxynonenal; IPGTT, intraperitoneal glucose tolerance test;
44 IPITT, intraperitoneal insulin tolerance test; FFA, free fatty acids; FBG, fasting blood
45 glucose; FINS, fasting serum insulin; HOMA-IR, homeostasis model
46 assessment-estimated insulin resistance; 2-NBDG,
47 2-deoxy-2-[(7-nitro-2,1,3-benzoxadiazol-4-yl) amino]-D-glucose; NQO1,
48 NAD(P)H:quinone oxidoreductase-1; HO-1, heme oxygenase 1; IL-1β, interleukin-1
49 β; Il-6, interleukin-6; TNF-α, tumor necrosis factor-α; CYP7a1, cholesterol
50 7α-hydroxylase; BAAT, bile acid-CoA:amino acid N-acyltransferase; 7α/β-HSDH,
51 7α/β-hydroxysteroid dehydrogenase.

52

53 **Introduction**

54 The prevalence of obesity and overweight have been on the rise worldwide[1].
55 Current predictions indicate that more than 1 billion people will be obese by 2030[2].
56 Visceral obesity precedes the development of metabolic complications and chronic
57 diseases such as type 2 diabetes mellitus (T2DM)[3], hepatic steatosis[4] and
58 cardiovascular diseases[5]. Metformin has been the first-line anti-diabetic drug for more
59 than 60 years because of its excellent hypoglycemic effect and safety profile[1].
60 Although several studies have explored the mechanisms by which metformin
61 maintains glucose homeostasis, findings from such studies are inconsistent. The
62 prevailing view is that metformin activates AMP-activated protein kinase (AMPK) in
63 the liver, similar to the principle of caloric restriction that relieves symptoms of
64 diabetes[6]. However, metformin is an orally administered drug that reaches high
65 concentrations in the intestine with much lower serum concentrations[7], thus, the
66 possibility that its metabolic therapeutic mechanism might be due in part to actions in
67 the intestine cannot be ignored. Accumulated evidence shows that a high-fat diet
68 (HFD) reduces the abundance of *Lactobacilli* in the small intestine. However, this can
69 be counteracted by metformin, which increases the proportion of probiotics, thus,
70 relieving the symptoms of HFD-induced diabetes[8]. Although metformin may play a
71 hypoglycemic effect by improving the gut microbiota, oral administration of
72 antibiotics to diabetic mice impairs the hypoglycemic ability of metformin[9]. In
73 addition, while metformin can increase the abundance of *Escherichia coli*, it can as

74 well reduce the abundance of *Intestinibacter*[10]. This can further influence diverse
75 biological processes such as the synthesis of branched-chain amino acid and the
76 secretion of GLP-1, thereby improving glucose tolerance and alleviating insulin
77 resistance (IR)[10,11]. These findings suggest that modulation of gut microbiota is
78 involved in the hypoglycemic mechanism of metformin.

79 Bile acids (BAs), which are produced in the liver and serve as important
80 ingredients of the digestive fluid in the intestine, enter the small intestine through the
81 biliary system and participate in fat digestion and absorption[12]. Gathered evidence
82 demonstrates that BAs could improve the intestinal homeostasis by modulating the
83 gut microbiota, thus relieving metabolic syndrome[13]. Recent studies also suggest that
84 BAs can participate in the liver-gut axis circulation and the improvement of
85 HFD-initiated metabolic disorders by inhibiting the proliferation of pathogenic
86 bacteria[14]. By modulating the gut microbiota, BAs have also been reported to induce
87 multiple beneficial effects on the intestinal lumen and intestinal walls such as the
88 suppression of intestinal inflammatory responses[15], the resolution of endoplasmic
89 reticulum (ER) stress in the intestinal epithelial cells underlying the pathology of
90 inflammatory bowel disease[16] and the improvement of gut barrier dysfunction[17-19].
91 These findings suggest that there is a complex relationship among BAs, gut
92 microbiota and metabolic syndrome.

93 Previous studies have reported the association of BAs with oxidative stress,
94 which has been shown to treat metabolic dysfunction by acting as an endogenous

95 chemical chaperone to protect cells against ER stress[20]. Intestinal micro-environment
96 (including inflammation status, the function of the epithelial tight junction and gut
97 microbiota) plays an essential role in the progression of obese-induced IR[21]. The
98 presence of gut microbiota and BAs in the intestine may be closely associated with
99 intestinal metabolic state[22,23]. Analyses from metagenomic sequencing and
100 metabolomics show that metformin treatment increases the levels of the conjugated
101 bile acid in the gut by decreasing the abundance and bile salt hydrolase (BSH) activity
102 of *Bifidobacterium* species in the intestines of individuals with T2DM[24,25]. BAs are
103 signal molecules that control the dynamic balance between energy metabolism and
104 liver protection. It has been reported that BAs change with obesity, IR[26] and
105 nonalcoholic steatohepatitis (NASH)[27]. However, the mechanism by which BAs
106 alleviate HFD-induced IR and the underlying role played by the gut microbiota during
107 this process are not clear.

108 Accumulating evidence has clearly indicated that oxidative stress plays a major
109 role in the pathological process of IR[28]. What's more, mitochondrial dysfunction,
110 reactive oxygen species (ROS) over production, and lipid peroxidation have been
111 found in the liver of Zucker rats with T2DM[29]. Increased oxidative stress seems to be
112 a deleterious factor leading to IR and impaired glucose tolerance in T2DM[30]. Nuclear
113 factor-erythroid-2-related factor 2 (Nrf2), tightly interacts with Kelch-like
114 ECH-associated protein 1 (KEAP1), an important transcription factor responsible for
115 inducing phase II detoxifying and antioxidant enzymes, is a key player in the

116 antioxidant response and glucose metabolism[31,32]. Recent study has confirmed
117 KEAP1-Nrf2 system as a critical target for preventing the onset of IR[33], and bile acids
118 have a great influence on the Nrf2/ARE antioxidant signal pathway[34]. This study
119 investigated how metformin prevents the development of IR in HFD-induced obese
120 mice by modulating the dysbiosis of gut microbiota and alteration metabolites.
121 Exploring the mechanism behind this improves our knowledge of gut microbiota and
122 metabolic interactions underlying the anti-insulin resistance effects of metformin.
123

124 **Results**

125 **1. Metformin alleviates HFD-induced insulin resistance and oxidative stress**

126 The administration of metformin significantly alleviated diet-induced increase of
127 body weight (**Fig. 1A)**, without affecting food intake (**Fig. S1A**). The reduced liver
128 index and subcutaneous fat index (**Fig. S1B)** as well as H&E staining of subcutaneous
129 adipose tissue (**Fig. S1C)** and number of adipocytes (**Fig. S1D)** suggested that
130 metformin prevented fat deposition in HFD-fed mice. The diet-induced dyslipidemia
131 was effectively prevented by metformin as indicated by the lower levels of T-CHO,
132 TG and FFA in both the liver and the serum (**Fig. S1E-G**). Further, metformin
133 significantly improved HFD-feeding impaired glucose tolerance and insulin resistance
134 determined by IPGTT (**Fig. 1B)** and IPITT (**Fig. 1C)**, respectively. Marked elevation
135 in fasting serum insulin (FINS) was observed in the HFD group. Notably, metformin
136 treatment tended to reverse the increase in FINS (**Fig. 1D**) as well as reduce

137 HOMA-IR (**Fig. 1E**), an indicator for evaluating the level of insulin resistance. In
138 addition, the level of phosphorylated Akt at Ser473 was significantly reduced in the
139 liver of the HFD-induced obese mice, but the level was restored in the HFD+Met
140 group (**Fig. 1F**). Contrary to the phosphorylated Akt, the level of phosphorylated
141 IRS-1 at Ser307 was significantly elevated in the HFD group, whereas this level was
142 reduced in the HFD+Met group (**Fig. 1F**). These results indicate that the preventive
143 effect of metformin on HFD-induced obesity resulted in improved glucose
144 homeostasis and insulin sensitivity.

145 Accumulated evidence indicated that oxidative stress is involved in the
146 development of HFD- induced IR, thus we further measured the oxidative stress
147 levels after metformin treatment. The results showed that the activity of CAT in the
148 serum and the liver was markedly lower in the HFD group compared with the NCD
149 group (**Fig. 2A**), the ratio of GSH/GSSG was also reduced (**Fig. 2B**). After metformin
150 intervention, the activity of CAT and the ratio of GSH/GSSG were significantly
151 increased. The accumulation of lipid peroxide MDA in liver, caused by HFD, was
152 significantly reduced in the metformin group (**Fig. 2C**). Nrf2/ARE is a classic
153 antioxidant-signaling pathway and KEAP1 is a key protein that mediates the
154 degradation of Nrf2. HFD feeding significantly inhibited Nrf2/ARE signaling
155 whereas metformin significantly increased the expression of Nrf2 as well as
156 phosphorylated Nrf2 (**Fig. 2D**). Nrf2/ARE signaling regulates the expression of a
157 variety of detoxification and antioxidant enzymes. As shown in **Fig. 2E**, Metformin

158 significantly up-regulated the mRNA levels of *Nqo1* and *Ho1*, which are essential
159 genes for balancing oxidative stress. Also, metformin prevented metabolic
160 inflammation in the liver and ileum, leading to a reduced gene expression of *Il-1β*,
161 *Il-6* and *Tnf-α* in the ileum (**Fig. S2A,B**). Metformin also prevented the release of
162 endotoxin LPS in serum (**Fig. S2C**). Meanwhile, the phosphorylated levels of p65 and
163 IκB were decreased in the livers of metformin-treated mice compared with the
164 HFD-fed mice (**Fig. S2D**), suggesting that the HFD-induced activation of NF-κB
165 signaling was suppressed by metformin. These results indicate that metformin can
166 improve HFD-induced insulin resistance, oxidative stress and inflammation.

167 **2. Metformin prevents obesity-driven dysbiosis of gut microbiota and reshapes**
168 **intestinal metabolites**

169 Faecal samples were collected for gut microbiota analysis by 16S rRNA
170 amplicon sequencing. Following all quality trimming and checking, three dataset with
171 highly qualified reads were collected for subsequent analysis. Our data showed that
172 the numbers of unique OTUs in the NCD, HFD, and HFD+Met groups were 372, 350
173 and 374, respectively. The coverage of sequencing results was nearly complete for all
174 sequences in the three groups, demonstrating sufficient sequencing depth for
175 follow-up analyses. The metformin-treated group significantly increased the Ace and
176 Chao1 indices compared with the HFD group (**Table 1**). Metformin-treated mice,
177 however, clustered partially apart from HFD-fed mice samples, suggesting important
178 changes in gut microbial profile (**Fig. 3A, Fig. S3A**). Metformin treatment prevented

179 HFD-induced decrease in Bacteroidetes and the increase in the
180 Firmicutes/Bacteroidetes ratio (**Fig. S3B,C**), two hallmarks of obesity-driven
181 dysbiosis. Based on FunGuild and FAPROTAX analysis of flora function, the HFD
182 group showed a decrease in the proportion of the chemoheterotrophy and the
183 fermentation bacteria when compared with the NCD group (**Fig. S3D**). However,
184 metformin supplementation reshaped the structure of gut microbiota,
185 chemoheterotrophy and fermentation improved in the HFD+Met group. Heatmap
186 presents the clustering of bacterial communities with their relative abundances at the
187 genus level (**Fig. 3B)**. Compared with the NCD group, unique high-abundance
188 bacteria in the HFD group are mainly concentrated in *Bifidobacterium, Roseburia,*
189 *Lachnoclostridum, Alloprevotella* and *Mucispirilum*. However, metformin decreased
190 the abundance of these bacteria, making the metformin-treated group comparable to
191 the NCD group. In addition, metformin specifically increased the abundance of
192 *Butyricimonas, Parasulterella, Parabacteroides* and *Akkermansia*. Consistent with
193 the decrease in Firmicutes/Bacteroidetes ratio, the difference between the HFD group
194 and the HFD+Met group is mainly reflected in the decrease in the abundance of
195 Firmicutes and the increase in the abundance of Bacteroidetes (**Fig. S3E**). Compared
196 with the NCD and HFD+Met groups, *c_Erysipelotrichia, f_proteobacteria,*
197 *g_Turicibacter, o_Bifidobacteriales* and *s_Clostridium* in the HFD group were
198 significantly up-regulated, whereas f*_Muribaculaceae, g_parabacteroides* and
199 *f_tannerellaceae* were significantly up-regulated in the HFD+Met group. Therefore,

200 metformin can increase the abundance of Bacteriodia at the phylum level and
201 *Akkermansia* at the genus level, and modulate HFD-induced dysbiosis of gut
202 microbiota.

203 The intestinal metabolite profiles were further measured using lipid
204 chromatography and mass spectrometry (LC-MS) to reveal the influences of
205 metformin on the intestinal metabolites. Metformin caused differential changes of
206 intestinal metabolites in HFD-fed mice evidenced by the scatter plots of OPLS-DA
207 (**Fig. 3C**). Compared to HFD group, metformin up-regulated 182 of intestinal
208 metabolites and down-regulated 118 metabolites in the HFD+Met group (**Fig. S4A**).
209 A total of 85 significantly differential metabolites between HFD and HFD+Met
210 groups were shown in **Fig. 3D**. The HFD+Met group effectively increases the content
211 of taurine, choline and TUDCA in the intestine compared with the HFD group (**Fig.**
212 **S4B)**. To further determine the source of TUDCA, the TUDCA content both in serum
213 and liver was detected. We found that TUDCA in the serum and liver of the
214 HFD+Met group was significantly increased compared with that in the HFD group
215 (**Fig. S4C)**. In the HFD+Met group, the gene expression of *Cyp7a1* and *Baat*, the
216 important enzymes involved in the biosynthesis of TUDCA, was significantly
217 up-regulated compared with that in the HFD group (**Fig. S4D**). In addition, BSH
218 secreted by *Bifidobacterium* and *Lactobacillus* could degrade the conjugated bile
219 acids, such as TUDCA. The relative abundance of these two bacteria was
220 significantly reduced in the HFD+SFF group compared to that in the HFD group, with

221 a concomitant reduction both in content (**Fig. 3E**) and activity (**Fig. 3F**) of BSH. It is
222 noteworthy that the reduced BSH activity was not caused by metformin (**Fig. 3G**).

223 **Fig. 4A**,**B** showed the correlation between intestinal metabolism and the gut
224 microbiome at the phylum and species level, respectively, after the intervention of
225 metformin in HFD-fed mice. TUDCA was highly associated with *A. muciniphila*
226 species belonging to the *Verrucomicrobia* phylum. Interestingly, through the analysis
227 of growth curves, it was not metformin but TUDCA significantly accelerated the
228 proliferation of *A. muciniphila in vitro* (**Fig. 4**C). These data suggest that metformin
229 may indirectly improve insulin resistance caused by a high-fat diet through
230 modulation of the intestinal abundance of *A. muciniphila* and content of TUDCA.

231 **3. TUDCA improves palmitic acid (PA)-induced insulin resistance and lipid**
232 **peroxidation**

233 Further study was carried out to determine whether TUDCA could alleviate
234 hepatic insulin resistance using a PA-treated HepG2 cell model. PA exposure (200
235 μM) resulted in a decrease in glucose uptake of HepG2 cells, demonstrated by the
236 reduction of fluorescence density in the cytoplasm (**Fig. 5A**) and the high
237 concentration of glucose in the medium (**Fig. 5B**). In addition, PA decreased the level
238 of phosphorylated Akt at Ser473 and increased phosphorylated IRS-1 at Ser307 (**Fig.**
239 **5C**), thus, revealing a typical symptoms of insulin resistance. As shown in **Fig. 5A,B**,
240 the impaired glucose uptake caused by PA was significantly alleviated by TUDCA,
241 excluding choline and taurine (**Fig. S5A-C**). Moreover, the suppressed

242 phosphorylation level of Akt in PA-treated HepG2 cells was elevated by TUDCA,
243 while the phosphorylated IRS-1 at Ser307 was also significantly reduced (**Fig. 5C**).
244 Consistent with the above results, in primary mouse hepatocytes, the PA-imparied
245 glucose uptake was also effectively alleviated and the phosphorylated Akt was
246 increased by TUDCA (**Fig. 5D-F**). These findings confirmed that TUDCA could
247 improve hepatic glucose intolerance and enhance insulin sensitivity of PA-treated
248 hepatocyte.

249 Homeostasis imbalances on glucose metabolism often cause inflammation and
250 oxidative stress damage in hepatic cells. Thus, we further investigated whether
251 TUDCA could alleviate these pathological processes. As shown in **Fig. 6A,** PA could
252 increase ROS generation in primary mouse hepatocytes and HepG2 cells, while
253 TUDCA significantly decreased PA-induced ROS production. On the other hand, the
254 ratio of GSH/GSSG was significantly increased by TUDCA (**Fig. 6B**). In addition,
255 pro-inflammatory cytokines such as *Tnf-α*, *Il-1β* and *Il-6* were also significantly
256 reduced by TUDCA treatment at mRNA level (**Fig. S6**).

257 We further investigated whether TUDCA alleviates PA-induced insulin
258 resistance through the Nrf2/ARE signaling pathway. The transcriptional activity of
259 Nrf2 was determined by measuring the mRNA levels of its representative downstream
260 target genes. TUDCA significantly up-regulated the expression of Nrf2 as well as its
261 phosphorylation level, suppressed by PA (**Fig. 6C, Fig. S7**). It also up-regulated the
262 expression of antioxidant genes, *Ho-1*, *Nqo1*, and *Gpx4*, downstream of the Nrf2/ARE

263 signaling pathway (**Fig. 6D**). We found that TUDCA was unable to alleviate
264 PA-impaired glucose uptake in HepG2 cells that interfered with Nrf2 expression, as
265 well as the primary hepatocytes from Nrf2 knockout mice (**Fig. 6E,F, Fig. S8A,B**).
266 The physical interaction between Nrf2 and KEAP1 was reduced by TUDCA (**Fig.**
267 **6G**), suggesting that TUDCA potentially antagonizes with KEAP1 to keep Nrf2 from
268 protein degradation by ubiquitination-proteasome. Binding to the Kelch domain of
269 KEAP1 to achieve the inhibition of KEAP1-Nrf2 interaction is a well-documented
270 mechanism for Nrf2 activation, thus the molecular docking analysis was performed to
271 explore the interaction between TUDCA and the Kelch domain of KEAP1. The
272 theoretical three-dimensional binding mode of the complex with the lowest docking
273 energy is illustrated in **Fig. 6H**. The simulation results revealed that TUDCA was able
274 to interact with the primary amino acid residues on the active site of KEAP1. TUDCA
275 was positioned at the hydrophobic pocket, surrounded by the residues Val-418,
276 Leu-557, Val-514, Val-561, and Thr-560, forming a stable hydrophobic binding. All
277 those interactions helped TUDCA to anchor in the binding site of KEAP1, and the
278 estimated binding energy of KEAP1-TUDCA complex was found to be −10.21
279 kcal/mol. The docking simulation provided supportive evidence for TUDCA induced
280 Nrf2 activation by allowing us to predict the binding site in Kelch domain.

281 Further, *ob/ob* mice were employed to validate the effect of TUDCA in
282 alleviating insulin resistance and lipid accumulation *in vivo*. Compared with *ob/ob*
283 mice without treatment, the *ob/ob* mice administrated with TUDCA showed

284 remarkable decrease in body weight, FBG, FINS, as well as HOMA-IR (**Fig. 7A-E**).
285 TUDCA treatment substantially restored glucose intolerance (**Fig. 7F-I**) and insulin
286 resistance (**Fig. 7J**) in *ob/ob* mice. Moreover, similar to WT mice, *ob/ob* mice
287 received TUDCA showed significant amelioration of total cholesterol and triglyceride
288 both in serum and liver (**Fig. S9A,B**). TUDCA significantly improved Nrf2
289 translocation into the hepatic nucleus (**Fig. 7J**), and up-regulated its downstream
290 antioxidant genes *Nqo1* and *Ho-1* (**Fig. 7K**), suggesting that the Nrf2/ARE signaling
291 pathway was activated by TUDCA. In addition, the abundance of *A. muciniphila* in
292 *ob/ob*+TUDCA group was significantly increased compared to *ob/ob* group (**Fig. 7L)**.
293 The gene experssion of pro-inflammatory factors (*Il-1β, Il-6,* and *Tnf-α*) in ileum were
294 also decresed in *ob/ob*+TUDCA group (**Fig. S9C**). Together, these results suggest
295 that TUDCA may significantly activate the Nrf2/ARE signaling, thereby enhancing
296 antioxidant and anti-inflammatory capacity as well as alleviating insulin resistance *in*
297 *vitro* and *in vivo*.
298

299 **Discussion**

300 Metabolic syndromes such as obesity, NAFLD and T2DM are increasingly
301 prevalent globally, especially in recent decades[2]. Metformin, the most widely used
302 anti-diabetic drug worldwide, has been reported to favorably influence metabolic and
303 cellular processes, alleviate insulin resistance[3,4]; however, the mechanism is still not
304 clear. Recent studies have revealed that the development of metabolic disease

305 strongly correlates to gut microbiota and metabolites. Multiple studies have
306 investigated the impact of metformin on gut microbiota, metabolites and related host
307 targets which regulate glucose metabolism[35]. We explored the potential mechanism
308 involving the gut microbiota and intestinal metabolites to reveal how metformin
309 improves diet-induced obesity and insulin resistance. We established that the daily
310 administration of metformin strongly ameliorated the obesity-related interruption of
311 gut microbiota. The bile acid TUDCA was maintained at a high level in the intestine,
312 which in turn promoted the proliferation of *A. muciniphila*, improved the integrity of
313 the intestinal wall and reduced intestinal inflammation. Furthermore, TUDCA was
314 identified as an activator of Nrf2/ARE signaling in hepatocyte that decreased
315 oxidative stress imbalance, while improving hepatic inflammation and insulin
316 resistance.

317 There is a variety of microbiota in the human intestine, which is involved in
318 body immunity, infection and nutrient metabolism, and they are closely associated
319 with the occurrence of diabetes. The gut microbiota imbalance in composition and
320 diversity can result in the release of bacterial endotoxin. This could lead to chronic
321 inflammation and destruction of the normal physiological functions of tissues and
322 organs. Several studies have confirmed that chronic inflammation can cause insulin
323 resistance and subsequently diabetes. The decrease in Firmicutes/Bacteroidetes ratio
324 is considered to be an indicator of improved metabolism by metformin therapy[35,36].
325 LDA analysis showed that the decreased abundance of Firmicutes by metformin could

326 be due to the decrease in *Erysipelotrichia* species, which belongs to the Firmicutes
327 phylum. The role of *Erysipelotrichia* species in human disease may be well
328 established in studies investigating metabolic disorders[37]. For instance, a previous
329 study showed a bloom of species belonging to the *Erysipelotrichaceae* family
330 (initially classified as *Mollicutes*) in diet-induced obese animals[38]. Within the host,
331 *Erysipelotrichia* species appear to be highly immunogenic[39], however, in surplus, they
332 induce intestinal inflammation. Studies have shown that species in
333 *Erysipelotrichaceae* are positively correlated with TNFα and IL-6 in the intestine and
334 the liver[40].

335 In contrast, most of the bacteria up-regulated by metformin were probiotics. For
336 example, species in *Muribacaceae* are involved in the L-citrulline nitrogen metabolic
337 cycle. They scavenge free radicals, improve immunity and maintain blood glucose.
338 Metformin also up-regulates the abundance of *Parabacteroides*, including *P.*
339 *distasonis* and *P. goldsteinii*. Liu et al.[41] found that *P. distasonis* could transform bile
340 acids, activate intestinal gluconeogenesis through succinic acid and improve the host
341 metabolic disorders. In another study, Wu et al.[42] recorded that *P. goldsteinii* reduces
342 systemic inflammation and increases insulin sensitivity by maintaining intestinal
343 integrity. *Akkermansia muciniphila* is known to effectively alleviate intestinal
344 inflammation caused by obesity[43]. Patients with intestinal obesity have been shown to
345 have a significantly reduced abundance of *A. muciniphila* compared with healthy
346 individuals. Numerous studies have demonstrated that metformin could up-regulate

347 the abundance of *A. muciniphila* in HFD-fed mice intestine, maintain the integrity of
348 the intestinal wall as well as effectively improve intestinal inflammation[44]. The
349 abundance of *A. muciniphila* is also significantly up-regulated in the HFD + Met
350 group. As a mucin-degrading bacterium, the use of *A. muciniphila* has been shown to
351 reduce inflammation, maintain the intestinal barrier and increase levels of
352 endocannabinoids secreted by intestinal peptides[45]. We speculate that the
353 transformation of gut microbiota by metformin is the defining factor in improving
354 chronic inflammation in the intestine and even the whole body. Metformin can
355 effectively inhibit the number of pathogenic bacteria and promote the proliferation of
356 probiotics. A suppression of pathogenic bacteria coupled with a proliferation of
357 probiotics may synergistically reduce intestinal inflammation and maintain the
358 integrity and permeability of the intestinal wall. Furthermore, this may lead to a
359 decrease in serum LPS and improvement of systemic inflammation caused by
360 HFD-induced obesity.

361 The "dialogue" between the gut microbiota and the organism mainly depends on
362 microbial metabolites. By producing various enzymes for biochemical metabolic
363 pathways of the intestinal microbes, gut microbiota can perform diverse metabolic
364 activities such as the metabolism of amino acids, carbohydrates and bile acids, as well
365 as the formation of a co-metabolic relationship with the host. Bile acids produced by
366 the gut microbiota are essential in the regulation of glycolipids and energy. Studies
367 have shown that in human primary hepatocytes, bile acids promote the β-oxidation of

368 fatty acids by activating FXR[46] and up-regulate the expression of apolipoprotein CII
369 gene to reduce the triglyceride content in the liver[47].

370 In our present study, metabolomics data showed that TUDCA in the intestine of
371 HFD+Met group increased significantly. Previous studies revealed that metformin
372 treatment increased the levels of conjugated bile acid in the gut by decreasing the
373 abundance of *Bifidobacterium* and its bile salt hydrolase (BSH) activity in the
374 intestines of individuals with T2DM[14,25]. BSH, secreted by intestinal bacteria,
375 decomposes TUDCA in the intestine and metabolizes TUDCA to taurine and UDCA.
376 The data from gut microbiota showed that metformin reduced the intestinal bacterial
377 abundance of *Bifidobacterium* and *Lactobacillus* in the mice fed a high-fat diet, while
378 *Bifidobacterium* was the main BSH-producing bacterium. In addition, the content and
379 activity of BSH in the mouse intestine of HFD+Met group were significantly reduced,
380 which was not related to metformin treatment. We hypothesize that high levels of
381 TUDCA are caused by a reduction in BSH-producing bacteria due to the remodeling
382 of the gut microbiota by metformin. *In vitro*, TCDCA can be transformed into
383 TUDCA by 7α/β-hydroxysteroid dehydrogenase (7α/β-HSDH)[12]. Data from the gut
384 microbiota also revealed that metformin did not affect the abundance of *Eubacterium*
385 and *Clostridium*, the major 7α/β-HSDH-producing bacteria. Therefore, the increase of
386 TUDCA in the intestine is purportedly not due to the inhibitory effect of metformin
387 on BSH-producing bacteria. According to the biosynthesis of bile acids in liver, the
388 conjugated bile acid TUDCA can be generated in the liver through a series of

389 catalytic reactions and enzymes such as CYP7A1 and BAAT[12,18]. CYP7A1 is a
390 rate-limiting enzyme that catalyzes the breakdown of cholesterol into bile acids in the
391 liver[12], whereas BAAT is a vital enzyme that catalyzes the amidation reaction of
392 taurine and UDCA[48]. Interestingly, we found that the gene expressions of *Cyp7a1* and
393 *Baat* were significantly enhanced by metformin, which might further promote the
394 synthesis of TUDCA in the liver. Thus, we suppose that the increase of TUDCA in
395 the intestine might due to the hepatic biosynthesis by metformin treatment.

396 TUDCA has been shown to treat NAFLD by acting as an endogenous chemical
397 chaperone; to protect cells against ER stress and to reduce liver steatosis[20]. Moreover,
398 TUDCA can alleviate dextran sulfate sodium-induced colitis in mice[49]. *In vitro*, we
399 found that TUDCA antagonizes with KEAP1 to keep Nrf2 from protein degradation
400 to activate Nrf2/ARE signaling pathway. This is reminiscent of the expression pattern
401 of Nrf2, a crucial stress regulator to reduce ROS, which is a key factor in sensitizing
402 insulin signaling[30,50]. It has also been confirmed that up-regulation of the Nrf2
403 expression both by genetic manipulation and pharmacological interference, can
404 significantly decrease the content of ROS and ameliorate IR and T2DM[31-34]. In the
405 mice supplemented with metformin, the significant up-regulation in the expression of
406 *Nrf2* and its downstream target genes (*Gclc*, *Cat* and *Ho-1*) occurred, which further
407 alleviated IR and over-oxidation[51,52]. Conversely, the stress-resistant effect of
408 TUDCA was dramatically repressed by the inhibition of the Nrf2/ARE signaling. We
409 also found that TUDCA can effectively reduce the inflammation and oxidative stress

410 as well as decreasing the accumulation of lipid peroxide *in vitro* and *in vivo*. This
411 might be a novel mechanism for metformin in the treatment of insulin resistance and
412 diabetes.

413 Overall, in our present study, metformin was found to increase TUDCA by
414 reducing the production of BSH, which antagonized the interaction between KEAP1
415 and Nrf2, prevented Nrf2 degradation and promoted its nuclear translocation.
416 TUDCA activated Nrf2/ARE pathway and increased the gene transcription of
417 antioxidant enzyme, further reduced oxidative stress and sensitized insulin signaling.
418 The increase of TUDCA in the intestine corresponded to the increase in the
419 abundance of *A. muciniphlia.* Metformin remodeled the gut microbiota by promoting
420 probiotics such as *Muribacaceae,* and *Parabacteroides*, and inhibiting pathogenic
421 bacteria such as *Erysipelotrichia* and *Helicobacter*, which maintained intestinal
422 integrity and reduced inflammation. However, for a better understanding of the
423 crucial mechanisms involved in the long-term treatment with metformin in humans,
424 the role of the intestine-liver axis should be explored. Since TUDCA is a novel
425 effector molecule of metformin in the gut, plays an important role in alleviating
426 metabolic syndrome.

427

428 **Materials and methods**

429 **Chemicals and diet**

430 Metformin (purity ≥ 98%), choline (purity ≥ 98%), taurine (purity ≥ 99%) and

431 palmitic acid (PA, purity ≥ 99%) were obtained from Sigma-Aldrich (St. Louis, MO,
432 USA). Tauroursodeoxycholic acid (TUDCA, purity ≥ 99%) was purchased from
433 Selleck (Houston, Texas, USA). Both the normal chow diet (NCD, containing 10%
434 fat by energy) and high-fat diet (HFD, containing 60% fat by energy) were purchased
435 from Beijing HFK Bio-Technology Co., Ltd. (Beijing, China). Antibodies against Akt,
436 phospho-Akt (Ser473), IRS-1, phospho-IRS-1 (Ser307), KEAP1, GAPDH, lamin B1
437 and β-tubulin were obtained from Cell Signaling Technology (Beverly, MA, USA).
438 Nrf2, phospho-Nrf2 (Ser40), and 4-HNE were purchased from Abcam (Cambridge,
439 UK). Horseradish peroxidase (HRP)–conjugated secondary antibody was obtained
440 from Santa Cruz Biotechnology (Santa Cruz, USA).

441 **Animal experiments**

442 All male mice (ICR mice, 7 weeks old, body weight 25 ± 2 g; C57BL/6J mice, 7
443 weeks old, body weight 20 ± 2 g; *ob/ob* mice, 7 weeks old, body weight 40 ± 2 g;
444 $Nrf2^{-/-}$ mice, 7 weeks old, body weight 20 ± 2 g) were housed in ventilated cages
445 (three animals per cage) at the SPF facility of Wenzhou University under controlled
446 environmental conditions (temperature 22 ± 2°C; relative humidity 60–70%) with free
447 access to standard laboratory chow and tap water. The mice were maintained on a
448 regular 12/12 h light/dark cycle.

449 Mice were acclimatized to their environment for 1 week before the experiments.
450 Mice were randomly allocated into three groups (n = 9 for each group). A co-worker
451 blinded to the experimental protocol randomized animals into these groups. As for the

452 pharmacological activity of metformin, one group of ICR mice was fed with NCD
453 and the other two groups were fed with HFD. After 12 weeks of HFD feeding, one
454 group of HFD-fed mice was administered metformin (200 mg/kg body weight), once
455 daily (HFD+Met group) for 6 weeks, whereas the NCD-fed mice (NCD group) and
456 other group of HFD-fed mice (HFD group) were treated with an equal volume of
457 saline for 6 weeks. The whole study lasted 18 weeks, during which the body weight,
458 water consumption and food intake were measured every week. At week 18,
459 intraperitoneal glucose tolerance test (IPGTT) and intraperitoneal insulin tolerance
460 test (IPITT) were performed as previously described[1]. As for the pharmacological
461 activity of TUDCA, one group of *ob/ob* mice was administered TUDCA (300 mg/kg
462 body weight), whereas the wild-type C57BL/6J mice and *ob/ob* mice in the other two
463 groups were treated with an equal volume of saline for 8 weeks as control.

464 Fresh feces were collected and stored immediately at 80°C for subsequent
465 analysis. At the end of the trial, after overnight fasting for 12 h, blood samples were
466 collected, and serum was isolated by centrifugation at 1000 × *g* for 15 min at 4°C, and
467 stored at −80°C for further assay. Tissues, including the adipose tissue, liver and
468 ileum, were weighed; one portion of the tissues was fixed with 10% formaldehyde for
469 histological analysis, and the other portion was immediately frozen in liquid nitrogen
470 for further analysis.

471 Organ index were calculated by the following formula:

472 BMI = body weight (kg)/body length $(m)^2$

473 Liver index = wet weight of liver/bw* 100%

474 Kidney index = wet weight of kidney/bw* 100%

475 Pancreas index = wet weight of pancreas/bw* 100%

476 Subcutaneous fat index = wet weight of adipose tissue/bw * 100%

477 **Biochemical analysis**

478 Total cholesterol (T-CHO), triacylglycerol (TG), free fatty acids (FFA), fasting
479 blood glucose (FBG), fasting serum insulin (FINS), acid phosphatase (ACP), alkaline
480 phosphatase (AKP), alanine aminotransferase (ALT), aspartate aminotransferase
481 (AST), catalase (CAT), malondialdehyde (MDA), lipopolysaccharides (LPS) were
482 determined by biochemical kits purchased from Jiancheng Bioengineering Institute
483 (Nanjing, China). The bile salt hydrolase (BSH) content was determined by
484 biochemical kit purchased from Jianglia Bioengineering Institute (Shanghai, China).
485 The ratio of reduced glutathione (GSH) and oxidized glutathione (GSSG) were
486 determined by a GSH:GSSG kit (Jiancheng Bioengineering Institute, Nanjing, China).
487 Homeostasis model assessment-estimated insulin resistance (HOMA-IR) was
488 calculated using the following formula:

489 HOMA-IR = FBG (mmol/L) × FINS (mU)/22.5

490 **Hematoxylin and eosin staining**

491 Adipose tissue were fixed in 10% formaldehyde overnight, paraffin-embedded,
492 sectioned (4-μm thickness, 3–5 sections/specimen) and stained with hematoxylin and
493 eosin (H&E) for histological analysis. Digital images of H&E stained sections were

494 acquired with a Nikon Eclipse Ti microscope at ×400 magnifications (Ti-E/U/S,
495 Japan). Image J software (National Institutes of Health, USA) was used to count
496 adipocytes.

497 **Cell culture**

498 Human liver hepatocellular carcinoma (HepG2) cells were cultured in MEM
499 (Sigma, St. Louis, MO, USA) supplemented with 10% FBS, penicillin and
500 streptomycin. Cells were maintained in 5% CO_2 at 37°C.

501 **Isolation and culture of primary hepatocyte**

502 Male C57/B6J and Nrf2$^{-/-}$ mice (8 weeks old) were used for isolating primary
503 hepatocyte. Hepatocytes were isolated by a two-step collagenase perfusion technique.
504 Briefly, the inferior vena cava was cannulated with angiocatheter and the portal vein
505 was cut. The liver was perfused via the inferior vena cava with 100 mL of PBS at
506 37 ℃, followed by perfusion with 100 mL of collagenase type IV (Wellington) in
507 HBSS containing Ca^{2+} and Mg^{2+} (GIBCO). After the liver was digested, it was
508 dissected out and cut into small pieces and passed through a 100 μm strainer (Falcon).
509 Hepatocytes were separated from non-parenchymal cells by low-speed centrifugation,
510 and further purified by Percoll gradient centrifugation (50% v/v, Sigma). Cells were
511 plated at a density of 0.3×10^6 on 6-well collagen-coated plate. Hepatocytes were
512 allowed to recover overnight and experiments were started 24 h post isolation.

513 **siRNA transfection**

514 *Nrf2* was knocked-down by RNA interference (RNAi) using the following 19-bp

515 (including a 2-deoxynucleotide overhang) siRNAs (Origene, Beijing, China): *Nrf2*,
516 SR321100A-AUUGAUGUUUCUGAUCUAUCACUTT;
517 SR321100B-GUCAGUAUGUUGAAUCAGUAGUUTC;
518 SR321100C-CCAGUCUUCAUUGCUACUAAUCAGG. Stealth RNAi (Origene,
519 Beijing, China) was used as a negative control (siCont). For transfection, cells were
520 seeded on a six-well plate, grown to ~80% confluence and transfected with siRNA
521 duplexes using Lipofectamine 3000 (Invitrogen, Camarillo, CA, USA) according to
522 the manufacturer's recommendations. After incubation for 48 h, the expression level
523 of Nrf2 protein was detected by western blotting.

524 **Glucose uptake assay**

525 Glucose uptake assay was carried out according to the previous study with some
526 modifications[53]. Cells were plated at 1 x 10^4/well in 96-well plates and used at
527 subconfluence after 24 h of preincubation. For experiments, all culture medium was
528 removed from each well and replaced with 100 μM fluorescent
529 2-Deoxy-2-[(7-nitro-2,1,3-benzoxadiazol-4-yl) amino]-D-glucose (2-NBDG) in
530 serum-free medium and incubated for 30 min. Subsequently, cells were washed thrice
531 with PBS and then the fluorescence intensity was determined with a fluorescence
532 microplate reader (Ex/Em, 488/520 nm). The glucose concentration in the medium
533 supernatant was determined by a glucose detection kit (Jiancheng Bioengineering
534 Institute, Nanjing, China).

535 **Determination of ROS levels**

536 Intercellular ROS levels were measured using a ROS Assay Kit (Beyotime,
537 Shanghai, China) according to the manufacturer's protocol. In brief, the
538 dichlorodihydrofluorescein diacetate (DCFH-DA; 10 mM) supplied in the kit was
539 diluted to 10 μM in serum-free medium. Subsequently, cells were pretreated with
540 TUDCA (20 μM) for 2 hour at a density of 3×10^3/96-well. Next, 200 μM PA
541 solution was added and co-incubated for 24 hours. The supernatant was then replaced
542 with serum-free medium. The DCFH-DA solution (10 μM) was added to the cells for
543 30 minutes at 37°C, and they were then resuspended with PBS (0.1 mM) after
544 washing twice with the indicated inducers. Fluorescence intensity was detected using
545 a hybrid/multi-modereaders (BioTek instruments Inc., Vermont, USA) to determine
546 ROS levels.

547 **Quantitative RT-PCR**

548 Total mRNA was isolated from tissue samples using TRIzol reagent (TAKARA,
549 Tokyo, Japan) and was reverse-transcribed into cDNA using a high-capacity cDNA
550 reverse transcription kit (TAKARA, Tokyo, Japan) according to the manufacturer's
551 protocol. The mRNA levels were quantified with quantitative PCR (qPCR) using
552 SYBR Green (Qiagen, Hilden, Germany). Amplification was performed on a
553 LightCycler480 *q*RT-PCR system (Roche, Mannheim, Germany) under the following
554 reactions: 95°C for 15 min, followed by 40 cycles at 95°C for 10 s, 60°C for 20 s, and
555 72°C for 20 s. The relative mRNA levels of target genes were normalized to the
556 expression of β-actin calculated using $2^{-\Delta\Delta ct}$ method. The primer pairs used in this

557 study are listed in **Supplementary table**.

558 **Western blotting**

559 Samples were homogenized with ice-cold RIPA lysis buffer containing protease
560 and phosphatase inhibitors (Beyotime, Shanghai, China). The homogenates were
561 centrifuged at 10 000 × *g* for 20 min at 4°C to remove the insoluble tissue debris. The
562 protein concentration in the supernatant was determined using a BCA protein assay
563 kit (Beyotime, Shanghai, China). Equal amount of protein for each group were
564 denatured in boiling water for 5 min. Aliquots (40 μg) of protein samples were
565 subjected to 10% SDS-PAGE and transferred to PVDF membranes (Millipore,
566 Bedford, MA, USA). After blocking with 5% nonfat milk (dissolved in TBST) for 1 h,
567 the membranes were incubated with the indicated antibodies at 4°C overnight,
568 followed by incubation with the appropriate HRP-conjugated second antibodies for 1
569 h at room temperature. Chemiluminescent detection was performed using the ECL
570 Plus Western blotting reagent (TransStart, Beijing, China). Semi-quantitative analysis
571 for densitometry of each band was performed using ImageJ software.

572 **Co-immunoprecipitation**

573 For co-immunoprecipitation (Co-IP), the whole protein lysates prepared from
574 HepG2 cells were extracted in a RIPA lysis buffer. Briefly, cell lysates were
575 incubated with Nrf2 or KEAP1 antibodies for 2 h at room temperature, followed by
576 binding of antigen antibody complexes to protein A/G magnetic beads (Thermo
577 scientific, Rockford, USA) for 1 h. Then, the antigen/antibody immunocomplex was

578 stripped by boiling with 5× loading sample buffer for western blotting incubated with
579 KEAP1, Nrf2 and GAPDH antibodies.

580 **Methodologies of gut microbiota by 16S rRNA amplicon sequencing**

581 Sample preparation: Fæcal samples were freshly collected at week 16 and
582 immediately stored at -80°C. Total fecal DNA was extracted using CTAB/SDS
583 method. The V4 region of the 16S rRNA was amplified using the universal primers
584 515F and 806R. All PCR reactions were carried out with Phusion® High-Fidelity PCR
585 Master Mix (New England Biolabs), and the mixture PCR products were purified
586 with GeneJET Gel Extraction Kit (Thermo Scientific). Sequencing libraries were
587 generated using Ion Plus Fragment Library Kit (Thermo Scientific) following
588 manufacturer's recommendations. The library quality was assessed on the Qubit 2.0
589 Fluorometer (Thermo Scientific). At last, the library was sequenced on an Ion S5™
590 XL platform (Thermo Scientific) and 400 bp/600 bp single end reads were generated.

591 Data acquisition: Paired-end reads were merged using FLASH (V1.2.7), and the
592 Raw fastq files were processed by QIIME (version 1.7.0). Sequence analysis was
593 performed by Uparse software (v7.0.1001), and Sequences with ⩾ 97% identity
594 were assigned to the same Operational Taxonomic Units (OTUs).

595 Data analysis: To compare the compositional OTUs of the gut microbiota in each
596 group, a Venn diagram was constructed using R packages (version 3.1.0) as
597 previously documented. Mothur software packages (version V.1.30.1) were used to
598 calculate the value of Chao1, Ace, Simpson index and Shannon index for evaluation

599 of the community richness and community diversity. Pair-group method with
600 arithmetic means (UPGMA) clustering was generated using the average linkage and
601 conducted by QIIME software (V1.7.0). Linear discriminant analysis (LDA) was
602 carried out to determine the highly dimensional gut microbes and characteristics
603 associated with NCD mice, HFD mice and HFD+Met mice.

604 **Methodologies of non-targeted metabolome analysis**

605 Metabolites extraction from colon contents: Colon contents were added ddH2O
606 (4°C) and mixed. 100 mg of sample was extracted with 1000 μL of pre-cooled
607 methanol (-20°C). After centrifugation, the supernatant was evaporated and finally
608 dissolved in 400 μL methanol aqueous solution (1:1, 4°C). For the quality control
609 (QC) samples, 20 μL of extract was taken from each sample and mixed. These QC
610 samples were used to monitor deviations of the analytical results from these pool
611 mixtures and compare them to the errors caused by the analytical instrument itself.
612 And the rest of the samples were used for LC-MS detection.

613 UPLC Conditions: Chromatographic separation was accomplished in an Acquity
614 UPLC system equipped with an ACQUITY UPLC® HSS T3 (150 × 2.1 mm, 1.8 μm,
615 Waters) column maintained at 4°C. The temperature of the auto sampler was 4°C.
616 Gradient elution of analytes was carried out with 0.1% formic acid in water (A) and
617 0.1% formic acid in acetonitrile (B) at a flow rate of 0.25 mL/min. Injection of 5 μL
618 of each sample was done after equilibration. An increasing linear gradient of solvent
619 B (v/v) was used as follows: 0~1 min, 2% B; 1~9.5 min, 2%~50% B; 9.5~14 min,

620 50%~98% B; 14~15 min, 98% B; 15~15.5 min, 98%~2% B; 15.5~17 min, 2%.

621 Mass spectrometry conditions: The ESI-MS^n experiments were executed on the
622 Thermo LTQ Orbitrap XL mass spectrometer with the spray voltage of 4.8 kV and
623 -4.5 kV in positive and negative modes, respectively. Sheath gas and auxiliary gas
624 were set at 45 and 15 arbitrary units, respectively. The capillary temperature was
625 325°C. The voltages of capillary and tube were 35 V and 50 V, -15 V and -50 V in
626 positive and negative modes, respectively. The Orbitrap analyzer scanned over a mass
627 range of m/z 89-1000 for full scan at a mass resolution of 60000. Data dependent
628 acquisition (DDA) MS/MS experiments were performed with CID scan. The
629 normalized collision energy was 30 eV. Dynamic exclusion was implemented with a
630 repeat count of 2, and exclusion duration of 15 s.

631 Data processing: UPLC-QTOF-MS raw data were analyzed with MarkerLynx
632 Application Manager 4.1 (Waters Corp.). The matrix from UPLC-QTOF-MS was
633 introduced into SIMCA-P 11.0 software (Umetrics) and standardized to a mean of 0
634 and variance of 1, according to the formula [X - mean(X)]/ std (X), for multivariate
635 statistical analysis. The t test with false discovery rate correction was used to measure
636 the significance of each metabolite. Partial least-squared discriminant analysis
637 (PLS-DA) and orthogonal partial least-squared discriminant analysis (OPLS-DA)
638 were conducted to identify the metabolite discrimination between the two group
639 samples. Differential metabolites were defined with variable importance in the
640 projection (VIP) > 1.0 obtained from OPLS-DA and *P* values less than 0.05 obtained

641 from t test. Differential metabolites were tentatively identified by database matching,
642 i.e., Human Metabolome Database (HMDB) (http://www.hmdb.ca), Metlin
643 (http://metlin.scripps.edu), massbank (http://www.massbank.jp/), LipidMaps
644 (http://www.lipidmaps.org), mzclound (https://www.mzcloud.org). Heatmaps of
645 differential metabolites among all groups were obtained based on spearman
646 correlation and cluster analyses.

647 **Growth curve of *Akkermansia muciniphila***

648 *Akkermansia muciniphila* strain ATCC BAA-835 was purchased from the Beina
649 Biologicals, Inc. (Beijing, China). Bacteria were cultured in BHI medium in tubes at
650 37°C in an anaerobic chamber (Whitley A35 Workstation 2.5, Don Whitley Scientific,
651 UK). To acquire the growth curve of *A. muciniphila*, the medium in test tubes
652 supplemented with or without 10 mM metformin (or 20 μM TUDCA) was placed in
653 an anaerobic bag to eliminate oxygen for 24 h. The test tubes were then inoculated
654 with bacteria and incubated at 37°C in an anaerobic bag. The OD_{600} of the cultures
655 was measured every 3 hours.

656 **Determination of hepatic/serum TUDCA**

657 The contents of TUDCA in tissues were determined by high-performance liquid
658 chromatography (HPLC). Briefly, 200 mg of frozen tissue was homogenized with a
659 Qiagen TissueLyserII (Germantown, MD, USA) in 1 mL of PBS to prepare the tissue
660 homogenates. The impurities were removed through a 0.22 μm filter, then the filtrate
661 was precipitated by methanol and 10 μL of supernatant was analyzed using an Agilent

662 1290 HPLC system (Santa Clara, CA) equipped with a Hypersil ODS-2 column (5 μm,
663 4.6 × 250 mm; Waters, USA). The supernatant was detected at the wavelength of 210
664 nm, eluted with the mobile phase of 0.03 M phosphate buffer solution (pH 4.4) and
665 methanol (32:68, v/v) at a flow rate of 1.0 mL/min.

666 **Determination of bile salt hydrolase activity *in vitro***

667 The enzyme activity of BSH was determined using an amino acid chromogenic
668 method. Briefly, mouse faeces were collected and the faecal suspension was prepared.
669 10 μL of sample (containing 500 μg of protein) was incubated with 180 μL of sodium
670 phosphate buffer and 10 μL of TDCA (final concentration 10 mM) at 37°C for 30 min.
671 50 μL of the mixture was mixed with 50 μL of 15% TCA and centrifuged at 10,000g
672 for 10 min. Mix 20 μL of supernatant with 80 μL of water, add 1.9 mL of ninhydrin
673 (0.5 mL 1% ninhydrin, 1.2 mL glycerol, 0.2 mL 0.5 M citrate buffer, pH 5.5) and
674 boil for 15 min. Cool the reaction tube, measure the absorbance at 570 nm and
675 calculate the BSH enzyme activity by substituting the formula for the taurine standard
676 curve.

677 **Molecular docking analysis**

678 To investigate the probable binding of TUDCA to KEAP1 as the potential
679 inhibitor, the automated docking studies were carried out using AutoDock vina 1.1.2
680 package. The X-ray crystal structure of the human KEAP1 (PDB ID: 6LRZ) was
681 downloaded from RCSB Protein Data Bank. The 3D structure of TUDCA (ZINC ID:
682 3914813) was downloaded from ZINC. The AutoDockTools 1.5.6 package was

683 employed to generate the docking input files. The molecular docking simulation
684 protein of Keap1 was prepared by removing water molecules and bound ligands. The
685 binding site of the KEAP1 was identified as centre_x: −9.944, centre_y: −38.993, and
686 centre_z: 3.869 with dimensions size_x: 85, size_y: 85, and size_z: 85. The
687 best-scoring (i.e.,with the lowest docking energy) pose as judged by the Vina docking
688 score was chosen and further analyzed using PyMoL 2.4.0 software.

689 **Statistical analysis**

690 Statistical comparisons among experimental groups were analyzed by one-way
691 ANOVA and Duncan's multiple-comparison test using the SPSS software (Version
692 21.0. Armonk, NY: IBM Corp.). *P* values less than 0.05 were considered statistically
693 significant.

694

695 **Acknowledgements**

696 We gratefully thank Qiaojuan Li and Lingfeng Hou (Wenzhou University) for
697 their assistance in animal experiments. We gratefully thank Alan K Chang (Wenzhou
698 University) for helpful discussion and for revising the language of the manuscript.

699

700 **Financial support**

701 This work was financially supported by the National Natural Science Foundation
702 of China (81872952 and 41876197), the National Key Research and Development
703 Project (2018YFD0901503), the Science and Technology Program of Wenzhou

(ZY2019013).

Conflict of interest

The authors declare no conflict of interest.

Authors' contributions

Y.Z., Y.C., J.L, D.H., J.Z. and L.Y performed the research. H.T., Y.Z. and Y.G. designed this study. R.T. and M.W. provided technical assistance. H.T. and Y.Z. analyzed the data and wrote the manuscript. R.T. and Y.G. revised the manuscript. H.T. and Y.G. had primary responsibility for final content. All authors have read and approved the final manuscript.

716 **References**

717 1. Muoio DM, Newgard CB. Mechanisms of disease: Molecular and metabolic
718 mechanisms of insulin resistance and beta-cell failure in type 2 diabetes. *Nat. Rev.*
719 *Mol. Cell Bio.* 2008; 9: 193-205.

720 2. Estes C, Razavi H, Loomba R, Younossi Z, Sanyal AJ. Modeling the
721 epidemic of nonalcoholic fatty liver disease demonstrates an exponential increase
722 in burden of disease. Hepatology. 2018; 67(1): 123-133.

723 3. Shen J, Obin MS, Zhao L. The gut microbiota, obesity and insulin resistance.
724 *Mol. Aspec. Medic.* 2013; 34(1): 39-58.

725 4. Bäckhed F, Manchester JK, Semenkovich CF, Gordon JI. Mechanisms
726 underlying the resistance to diet-induced obesity in germ-free mice. *P. Natl. Acda.*
727 *Sci. USA*. 2007;104(3): 979-984.

728 5. Cho NH, Shaw JE, Karuranga S, Huang Y, Rocha Fernandes JD, Ohlrogge
729 AW, Malanda B. IDF diabetes atlas: global estimates of diabetes prevalence for
730 2017 and projections for 2045. *Diabetes Res. Clin. Pract.* 2018; 138: 271-281.

731 6. Zhou G, Myers R, Li Y, Chen Y, Shen X, Fenyk-Melody J, Wu M, Ventre J,
732 Doebber T, Fujii N, Musi N, Hirshman MF, Goodyear LJ, Moller DE. Role of
733 AMP-activated protein kinase in mechanism of metformin action. *J. Clin. Invest.*
734 2001; 108: 1167-1174.

735 7. Lee H, Ko G. Effect of metformin on metabolic improvement and gut
736 microbiota. *Appl. Enviro. Micorb.* 2014; 80: 5935-5943.

737 8. Zhang X, Zhao Y, Xu J, Xue ZS, Zhang MH, Pang XY, Zhang XJ, Zhao LP.
738 Modulation of gut microbiota by berberine and metformin during the treatment of
739 high-fat diet-induced obesity in rats. *Sci. Rep.* 2015; 5: 14405.
740 9. Zhou ZY, Ren LW, Zhan P, Yang HY, Chai DD, Yu ZW. Metformin exerts
741 glucose-lowering action in high-fat fed mice via attenuating endotoxemia and
742 enhancing insulin signaling. *Acta Pharmacol. Sin.* 2016; 37: 1063-1075.
743 10. Kristoffer F, Falk H, Trine N, Gwen F, Emmanuelle LC, Shinichi S, Edi P,
744 Sara VS, Valborg G, Helle KP, Manimozhiyan A, Karsten K, Anita YV, Henrik
745 V, Rajna H, Paul IC, Jens RK, Junhua L, Torben J, Florence L, Joël D, Søren B,
746 Jeroen R, Torben H, Jun W, Dusko ES, Peer B, and Oluf P. Disentangling the
747 effects of type 2 diabetes and metformin on the human gut microbiota. *Nature.*
748 2015; 528(7581): 262–266.
749 11. Pedersen HK, Gudmundsdottir V, Nielsen HB, Hyotylainen T, Nielsen T,
750 Jensen BA, Forslund K, Hildebrand F, Prifti E, Falony G, Le Chatelier E,
751 Levenez F, Doré J, Mattila I, Plichta DR, Pöhö P, Hellgren LI, Arumugam M,
752 Sunagawa S, Vieira-Silva S, Jørgensen T, Holm JB, Trošt K; MetaHIT
753 Consortium, Kristiansen K, Brix S, Raes J, Wang J, Hansen T, Bork P, Brunak S,
754 Oresic M, Ehrlich SD, Pedersen O. Human gut microbes impact host serum
755 metabolome and insulin sensitivity. *Nature.* 2016; 535(7612): 376-381.
756 12. Jia W, Xie GX, Jia WP. Bile acid-microbiota crosstalk in gastrointestinal
757 inflammation and carcinogenesis. *Nat. Rev. Gastroenterol Hepatol.* 2018; 15(2):

758 111-128.

759 13. Yao L, Seaton SC, Ndousse-Fetter S, Adhikari AA, DiBenedetto N, Mina AI,
760 Banks AS, Bry L, Devlin AS. A selective gut bacterial bile salt hydrolase alters
761 host metabolism. *eLife*. 2018; 17(7): e37182.

762 14. Sun LL, Xie C, Wang G, Wu Y, Wu Q, Wang XM, Liu J, Deng YY, Xia JL,
763 Bo C, Zhang SY, Chuyu Y, Lian G, Zhang XJ, Zhang H, Bisson WH, Shi JM,
764 Gao XX, Ge PP, Liu CH, Krausz WK, Nicholis RG, Cai JW, Rimal BP, Patterson
765 A, Wang X, Gonzalez FJ, Jiang CT. Gut microbiota and intestinal FXR mediate
766 the clinical benefits of metformin. *Nat. Med.* 2018; 24(12): 1919-1929.

767 15. Martínez-Moya P, Romero-Calvo I, Requena P, Hernández-Chirlaque C,
768 Aranda CJ, González R, Zarzuelo A, Suárez MD, Martínez-Augustin O, Marín JJ,
769 de Medina FS. Dose-dependent antiinflammatory effect of ursodeoxycholic acid
770 in experimental colitis. *Int. Immunopharmacol.* 2013; 15(2): 372–380.

771 16. Berger E, Haller D. Structure-function analysis of the tertiary bile acid
772 TUDCA for the resolution of endoplasmic reticulum stress in intestinal epithelial
773 cells. *Biochem. Biophys. Res. Commun.* 2011; 409: 610–615.

774 17. Stenman LK, Holma R, Gylling H, Korpela R. Genetically obese mice do not
775 show increased gut permeability or faecal bile acid hydrophobicity. *Br. J. Nutr.*
776 2013; 110: 1157–1164.

777 18. Arab JP, Karpen SJ, Dawson PA, Arrese M, Trauner M. Bile acids and
778 nonalcoholic fatty liver disease: Molecular insights and therapeutic perspectives.

779 *Hepatology*. 2017; 65: 350–362.

780 19. Wang WJ, Zhao JF, Gui WF, Sun D, Dai HJ, Xiao L, Chu HK, Fan D, Zhu
781 QJ, Bernd S, Huang K, Yang L, and Hou XH. Tauroursodeoxycholic acid inhibits
782 intestinal inflammation and barrier disruption in mice with non-alcoholic fatty
783 liver disease. *Brit. J. Pharmacol.* 2018; 175: 469–484.

784 20. Xie Q, Khaoustov VI, Chung CC, Sohn J, Krishnan B, Lewis DE, Yoffe B.
785 Effect of tauroursodeoxycholic acid on endoplasmic reticulum stress-induced
786 caspase-12 activation. *Hepatology.* 2002; 36(3): 592–601.

787 21. Fondevila C, Shen XD, Tsuchiyashi S, Yamashita K, Csizmadia E, Lassman
788 C, Busuttil RW, Kupiec-Weglinski JM, Bach FH. Biliverdin therapy protects rat
789 livers from ischemia and reperfusion injury. *Hepatology.* 2004; 40: 1333–1341.

790 22. Nakao A, Otterbein LE, Overhaus M, Sarady JK, Tsung A, Kimizuka K,
791 Nalesnik MA, Kaizu T, Uchiyama T, Liu F, Murase N, Bauer AJ, Bach FH,
792 Biliverdin protects the functional integrity of a transplanted syngeneic small
793 bowel. *Gastroenterology.* 2004; 127: 595–606.

794 23. Ester GS, Maria JP, Nikolaj SN, Oscar B, Maria JM, Elisa L, Maria AS, Jose
795 JGM. Protective role of biliverdin against bile acid-induced oxidative stress in
796 liver cells. *Free Radical Bio. Med.* 2016; 97: 466–477.

797 24. Zhang M, Feng R, Yang M, Qian C, Wang Z, Liu W, Ma J. Effects of
798 metformin, acarbose, and sitagliptin monotherapy on gut microbiota in Zucker
799 diabetic fatty rats. *BMJ Open Diab. Res. Ca.* 2019; 7(1): e000717.

800 25. Nova E, Pérez de Heredia F, Gómez-Martínez S, Marcos A. The Role of
801 Probiotics on the Microbiota: Effect on Obesity. *Nutr. Clin. Pract.* 2016; 31(3):
802 387-400.
803 26. Zhang WP, Chen LH, Feng H, Wang W, Cai Y, Qi F, Tao XF, Liu J, Shen
804 YJ, Ren XF, Chen X, Xu JM, Shen YX. Rifampicin-induced injury in HepG2
805 cells is alleviated by TUDCA via increasing bile acid transporters expression and
806 enhancing the Nrf2- mediated adaptive response. *Free Radical Bio. Med.* 2017;
807 112: 24–35.
808 27. Tangvarasittichai S. Oxidative stress, insulin resistance, dyslipidemia and
809 type 2 diabetes mellitus. *World J. Diabetes.* 2015; 6(3): 456–480.
810 28. Maiese K. New insights for oxidative stress and diabetes mellitus. *Oxid. Med.*
811 *Cell Longev.* 2015; 2015: e875961.
812 29. Raza H, John A, Howarth FC. Increased oxidative stress and mitochondrial
813 dysfunction in zucker diabetic rat liver and brain. *Cell Physiol. Biochem.* 2015;
814 35(3): 1241–1251.
815 30. Wan HWN, Kwak MK, Makpol S, Wan NWS, Mohd Yusof YA. Piper betle
816 induces phase I & II genes through Nrf2/ARE signaling pathway in mouse
817 embryonic fibroblasts derived from wild type and Nrf2 knockout cells, BMC
818 Complement. *Altern. Med*. 2014; 14: 72.
819 31. Uruno A, Yagishita Y, Yamamoto M. The Keap1-Nrf2 system and diabetes
820 mellitus. *Arch. Biochem. Biophys*. 2015; 566: 76–84.

821 32. Uruno A, Furusawa Y, Yagishita Y, Fukutomi T, Muramatsu H, Negishi T,
822 Sugawara A, Kensler TW, Yamamoto M. The Keap1-Nrf2 system prevents onset
823 of diabetes mellitus. *Mol. Cell Biol.* 2013, 33(15): 2996–3010.
824 33. Peng DF, Lu H, Zhu SM, Zhou ZJ, Hu TL, Chen Z, Zaika A, El-Rifai W.
825 NRF2 antioxidant response protects against acidic bile salts- induced oxidative
826 stress and DNA damage in esophageal cells. *Cancer Lett.* 2019; 458: 46–55.
827 34. Kamisako T, Tanaka Y, Kishino Y, Ikeda T, Yamamoto K, Masuda S,
828 Ogawa H. Role of Nrf2 in the alteration of cholesterol and bile acid
829 metabolismrelated gene expression by dietary cholesterol in high fat fed mice. *J.*
830 *Clin. Biochem. Nutr.* 2014; 54(2): 90–94.
831 35. Canfora EE, Meex R, Venema K, and Blaak EE. Gut microbial metabolites
832 in obesity, NAFLD and T2DM. *Nat. Rev. Endocrinol.* 2019; 15: 261–273.
833 36. Kaakoush NO. Insights into the Role of erysipelotrichaceae in the human
834 host. *Front. Cell. Infect. Microbiol.* 2015; 20: 84.
835 37. Turnbaugh PJ, Backhed F, Fulton L, and Gordon JI. Marked alterations in
836 the distal gut microbiome linked to diet-induced obesity. *Cell Host Microbe.*
837 2008; 3(4): 213–223.
838 38. Craven M, Egan CE, Dowd SE, McDonough SP, Dogan B, Denkers EY.
839 Inflammation drives dysbiosis and bacterial invasion in murine models of ileal
840 Crohn's disease. *PLoS ONE.* 2012; 7: e41594.
841 39. Ff

842 40.

843 41. Wang K, Liao MF, Zhou N, Bao L, Ma K, Zheng ZY, Wang YJ, Liu C,
844 Wang WZ, Wang J, Liu SJ, Liu HW. *Parabacteroides distasonis* alleviates
845 obesity and metabolic dysfunctions via production of succinate and secondary
846 bile acids. *Cell Rep.* 2019; 26(1): 222-235.

847 42. Wu TR, Lin CS, Chang CJ, Lin TL, Martel J, Ko YF, Ojcius MD, Lu CC,
848 Young DJ, Lai HC. Gut commensal *Parabacteroides goldsteinii* plays a
849 predominant role in the anti-obesity effects of polysaccharides isolated from
850 *Hirsutella sinensis*. *Gut.* 2019; 68(2): 248–262.

851 43. Anhê FF, Roy D, Pilon G, Dudonne S, Matamoros S, Varin T, Marette A. A
852 polyphenol-rich cranberry extract protects from diet-induced obesity, insulin
853 resistance and intestinal inflammation in association with increased *akkermansia*
854 *spp*. population in the gut microbiota of mice. *Gut.* 2015; 64(6): 872–883.

855 44. Chelakkot C, Choi Y, Kim DK, Park HT, Ghim J, Kwon Y, Jeon J, Kim MS,
856 Jee YK, Gho YS, Park HS, Kim YK, Ryu SH. *Akkermansia muciniphila*-derived
857 extracellular vesicles influence gut permeability through the regulation of tight
858 junctions. *Exp. Mol. Med*. 2018; 50(2): e450.

859 45. Everard A, Belzer C, Geurts L, Ouwerkerk JP, Druart C, Bindels LB, Guiot
860 Y, Derrien M, Muccioli GG, Delzenne NM, de Vos WM, Cani PD. Cross-talk
861 between Akkermansia muciniphila and intestinal epithelium controls diet-induced
862 obesity. *Proc. Natl. Acad. Sci. U S A.* 2013; 110(22):9066-9071.

863 46. Manley S, Ding WX. Role of farnesoid X receptor and bile acids in alcoholic
864 liver disease. *Acta Pharm. Sin. B.* 2015; 5(2): 158–167.
865 47. Kast HR, Nguyen CM, Sinal CJ, Jones SA, Laffitte BA, Reue K, Gonzalez
866 FJ, Willson TM, Edwards PA. Farnesoid X-activated receptor induces
867 apolipoprotein C-II transcription: a molecular mechanism linking plasma
868 triglyceride levels to bile acids. *Mol. Endocrinol.* 2001; 15(10):1720-1728.
869 48. Chiang YLJ. Bile acids: regulation of synthesis. *J. Lipid Res.* 2009; 50(10):
870 1955-1966.
871 49. Rodriguez J, Hiel S, Delzenne NM. Metformin: old friend, new ways of
872 action-implication of the gut microbiome? *Curr. Opin. Clin. Nutr. Metab. Care.*
873 2018; 21(4): 294-301.
874 50. Wible RS, Ramanathan C, Sutter CH, Olesen KM, Kensler TW, Liu AC,
875 Sutter TR. NRF2 regulates core and stabilizing circadian clock loops, coupling
876 redox and timekeeping in Mus musculus. Elife. 2018 Feb 26;7:e31656.
877 51. Sun CC, Lai YN, Wang WH, Xu XM, Li XQ, Wang H, Zheng JY, Zheng JQ.
878 Metformin Ameliorates Gestational Diabetes Mellitus-Induced Endothelial
879 Dysfunction via Downregulation of p65 and Upregulation of Nrf2. *Front*
880 *Pharmacol.* 2020; 11: e575390.
881 52. Abdelsamia EM, Khaleel SA, Balah A, Abdel Baky NA. Curcumin augments
882 the cardioprotective effect of metformin in an experimental model of type I
883 diabetes mellitus; Impact of Nrf2/HO-1 and JAK/STAT pathways. Biomed

884 Pharmacother. 2019; 109: 2136-2144.

885 53. Zou CH, Wang YJ, Zhen ZF. 2-NBDG as a fluorescent indicator for direct

886 glucose uptake measurement. *J. Biochem. Biophys. Methods.* 2005; 64: 207–215.

887

888 **Figure captions**

889 **Figure 1. Metformin prevents obesity and insulin resistance in HFD-fed mice.** (A)
890 Body weight was shown throughout 6 weeks. (B,C) Mice, fasted overnight and fasted
891 for 6 hours, were injected with glucose (2 g/kg in saline) or insulin (0.75 IU/kg in
892 saline) for IPGTT and IPITT, respectively. (B) IPGTT and (B') AUC of IPGTT; (C)
893 IPITT and (C') slope of IPITT. (D) FINS and (E) HOMA-IR. (F) Protein expression
894 of Akt, phosphorylated Akt at Ser473, IRS-1, phosphorylated IRS-1 at Ser307 and
895 quantitative analysis for the densitometry. Data are expressed as mean ± SD. *P <
896 0.05, **P < 0.01 and ***P < 0.001 for HFD *vs* HFD+Met. AUC, area under the curve;
897 FINS, fasting serum insulin; HOMA-IR, homeostatic model assessment for insulin
898 resistance; IPGTT, intraperitoneal glucose tolerance test; IPITT, intraperitoneal
899 insulin tolerance test; Met, metformin.

900 **Figure 2. Metformin ameliorates HFD-induced oxidative stress.** (A-C) Serum or
901 liver homogenate were used to quantify the representative of oxidative stress: (A)
902 CAT, (B) GSH:GSSG ratio, and (C) MDA. (D) Protein expression of total Nrf2,
903 phosphorylated Nrf2 and (D', D'') quantitative analysis for the densitometry. (E)
904 Quantitative RT-PCR analysis of *Nrf2*, *Keap1*, *Nqo1* and *Ho-1* are shown. Data are
905 expressed as mean ± SD. *P < 0.05, **P < 0.01 and ***P < 0.001 for HFD *vs*
906 HFD+Met. CAT, catalase; GSH, glutathione; GSSG, oxidized glutathione; MDA,
907 malondialdehyde.

908 **Figure 3. Genus-based comparison of gut microbiota and non-targeted**
909 **metabolome analysis.** (A) Principal coordinates analysis. (B) Heatmap showing
910 clustering of bacterial communities with their relative abundances at the genus level,
911 the bacterial communities or OTUs were clustered phylogenetically by
912 neighbor-joining method and the libraries were clustered by profile pattern using
913 Unifrac analysis. Relative abundances (log values) of microbial genus are displayed
914 in a red-to-blue color code (high to low abundance). (C) OPLS-DA score plot of
915 non-targeted metabolome. (D) Heatmap of 85 significantly differential metabolites. (E)
916 BSH content and (F) BSH activity in faeces of the three groups of mice. (G) Fecal
917 suspensions were prepared by collecting fresh faeces, adding metformin to final
918 concentrations of 5, 10 and 20 mg/mL, incubating for 30 min and then measuring
919 BSH activity. Data are expressed as mean ± SD. *$P < 0.05$, **$P < 0.01$ and ***$P <$
920 0.001 for HFD *vs* HFD+Met. PCoA, principal coordinates analysis; OPLS-DA,
921 orthogonal partial least-squared discriminant analysis; Met, metformin; BSH, bile salt
922 hydrolase.

923 **Figure 4. Correlation heatmap for gut microorganisms and metabolites.** (A-B)
924 The correlation coefficients of the differential metabolites and gut microbiota were
925 calculated by Pearson's algorithm using R language, and heat maps were created
926 based on the correlation coefficients. Matrix heatmap showing the correlation
927 between gut microbiota and metabolome at (A) Phylum and (B) Species levels,

928 respectively. (C) Growth curve of *A. muciniphila* in the presence of metformin or
929 TUDCA. Met, metformin; TUDCA, tauroursodeoxycholic acid.

930 **Figure 5. TUDCA alleviates insulin resistance in PA-treated hepatocytes.** (A-C)
931 HepG2 cells were pre-treated with 200 μM PA for 24 h and then incubated with
932 TUDCA (10 or 20 μM) for 12 h. (A) Glucose uptake and (B) glucose in the medium
933 supernatant. (C) Protein levels of p-Akt, Akt, p-IRS-1, IRS-1 and (C', C'') quantitative analysis for the densitometry. (D-F) Primary mouse hepatocytes were
935 pre-treated with 200 μM PA for 24 h and then incubated with TUDCA (10 or 20 μM)
936 for 4 h. (D) Glucose uptake and (E) glucose in the medium supernatant. (F) Protein
937 levels of p-Akt, Akt, p-IRS-1, IRS-1 and (F', F'') quantitative analysis for the
938 densitometry. Data are expressed as the mean ± SD. *$P < 0.05$, **$P < 0.01$ and ***P
939 < 0.001. PA, palmitic acid; TUDCA, tauroursodeoxycholic acid.

940 **Figure 6. TUDCA relieves PA-induced insulin resistance via activating**
941 **Nrf2/ARE signaling pathway.** (A) Intracellular ROS content; (B) ratio of
942 GSH/GSSG; (C) protein levels of p-Nrf2 and Nrf2 were determined by western
943 blotting in primary mouse hepatocytes and HepG2 cells. (D) Quantitative RT-PCR
944 analysis of *Nrf2*, *Ho-1*, *Nqo1* and *Gpx4* in primary mouse hepatocytes and HepG2
945 cells. Glucose uptake by cells and glucose content of the medium supernatant
946 measured in Nrf2 knock-down HepG2 cells (E) and primary hepatocytes from $Nrf2^{-/-}$
947 mice (F). (G) Immunoprecipitation. HepG2 cells were treated with or without
948 TUDCA, and then lysates were immunoprecipitated with the indicated antibodies,

949 followed by western blotting. (H) Docking of TUDCA with Kelch domain of KEAP1.
950 The residues of KEAP1 were represented using sticks or surface structures; TUDCA
951 was shown in pink; the dashed lines (blue) represent hydrogen-bonding interactions.
952 Data are expressed as mean ± SD. *$P < 0.05$, **$P < 0.01$ and ***$P < 0.001$. ROS,
953 reactive oxygen species; GSH, glutathione; GSSG, oxidized glutathione; PA, palmitic
954 acid; TUDCA, tauroursodeoxycholic acid.

955 **Figure 7. TUDCA improves obesity and insulin resistance in *ob/ob* mice.** (A-E)
956 Wild-type C57BL/6J mice and *ob/ob* mice was administered with or without TUDCA
957 for 8 weeks. (A) Body size, (B) body weight, serum levels of (C) FBG and (D) FINS,
958 (E) HOMA-IR. (F-I) Mice, fasted overnight and fasted for 6 hours, were injected with
959 glucose (2 g/kg in saline) or insulin (0.75 IU/kg in saline) for IPGTT and IPITT,
960 respectively. (F) IPGTT, (G) AUC of IPGTT, (H) IPITT and (I) slope of IPITT are
961 shown. (G) Protein expression of p-Akt, Akt, Nrf2 in nuclear and cytoplasm. (K)
962 Quantitative RT-PCR analysis of *Nqo1* and *Ho-1*. (L) Abundance of *A. muciniphila*.
963 Data are expressed as mean ± SD. *$P < 0.05$, **$P < 0.01$ and ***$P < 0.001$ for *ob/ob*
964 vs *ob/ob*+TUDCA. AUC, area under the curve; FBG, fasting blood glucose; FINS,
965 fasting serum insulin; HOMA-IR, homeostatic model assessment for insulin
966 resistance; IPGTT, intraperitoneal glucose tolerance test; IPITT, intraperitoneal
967 insulin tolerance test; TUDCA, tauroursodeoxycholic acid.

968

969 **Table 1. Diversity of gut microbiota in HFD and HFD+Met treated mice**

Groups	Reads	OTUs	Observed species	Ace	Chao1	Shannon	Simpson
NCD	78316±4945	372±35	330±21	345±17	350±21	5.10±0.67	0.92±0.04
HFD	76154±7745	350±40	312±20	325±24	326±24	5.38±0.33	0.95±0.02
HFD+Met	80004±421	374±21	335±20*	342±22*	348±20*	5.24±0.27	0.95±0.02

970 Data are expressed as mean ± SD. *$P < 0.05$ compared with HFD.

971

Figure 1

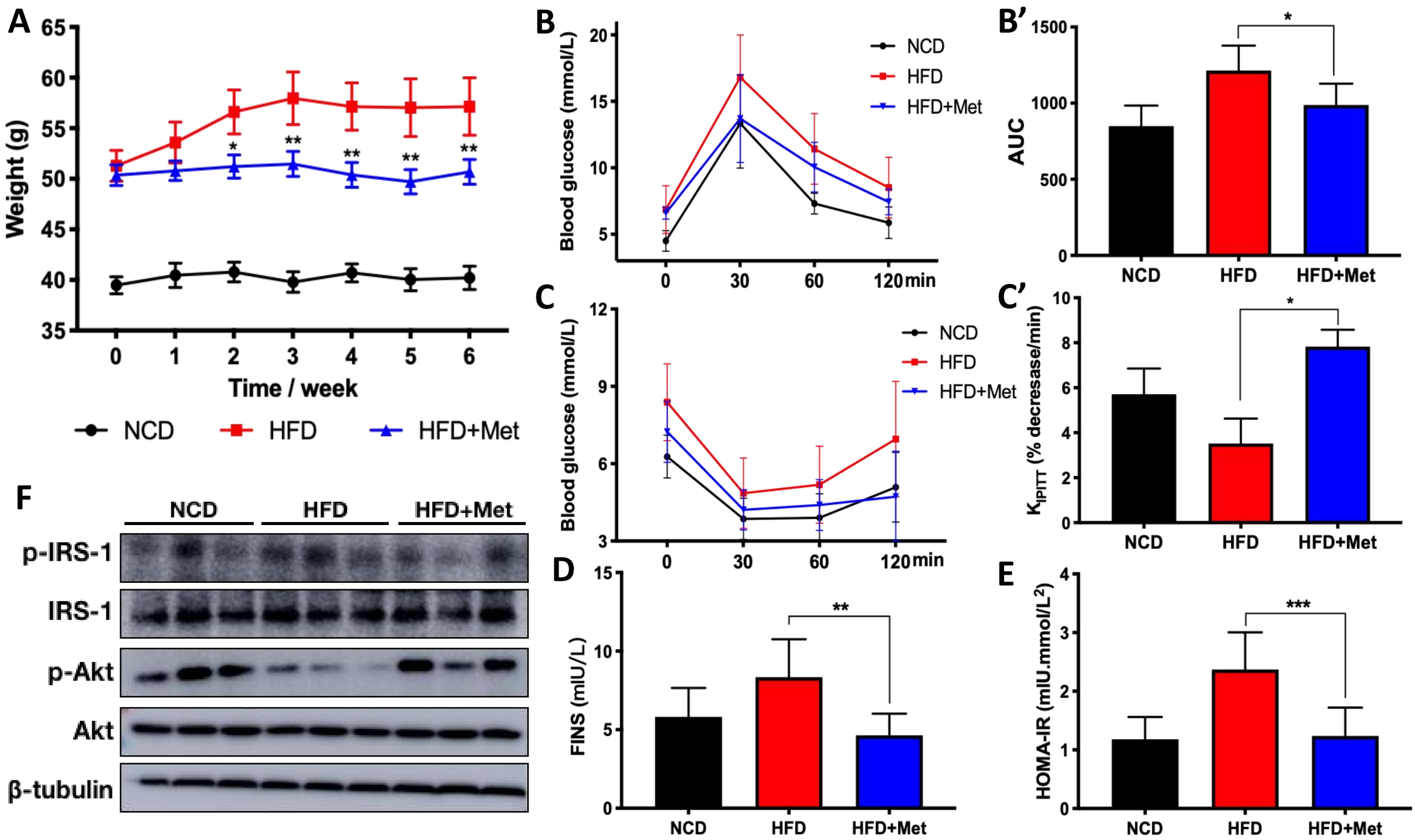
A
Weight (g)
Time / week
NCD
HFD
HFD+Met
B
Blood glucose (mmol/L)
120 min
B'
AUC
C
C'
K_{IPITT} (% decresase/min)
D
FINS (mIU/L)
E
HOMA-IR (mIU.mmol/L^2)
F
p-IRS-1
IRS-1
p-Akt
Akt
β-tubulin

Figure 2

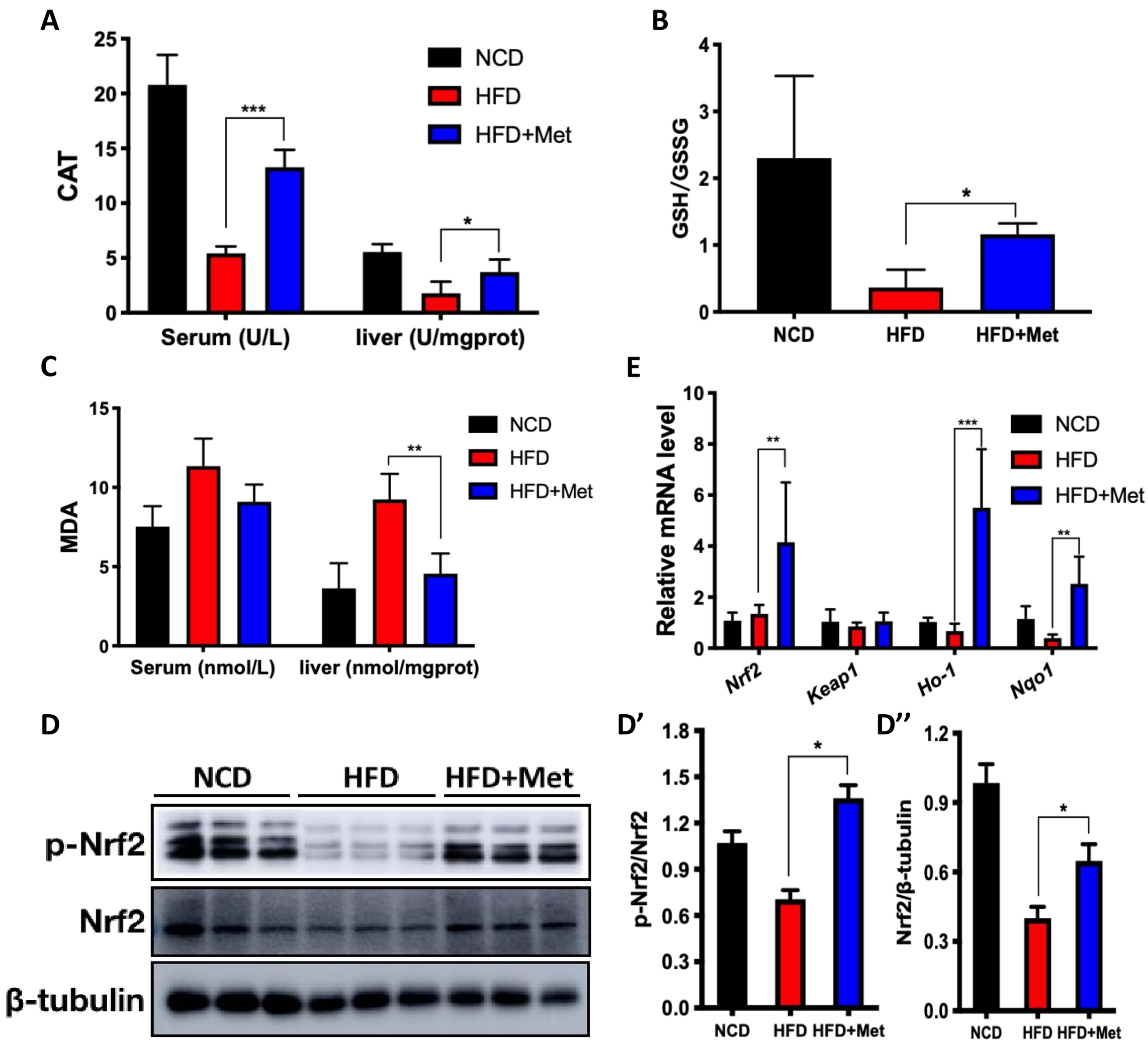
A
CAT
NCD
HFD
HFD+Met
***
*
Serum (U/L)
liver (U/mgprot)
B
GSH/GSSG
*
NCD
HFD
HFD+Met
C
MDA
NCD
HFD
HFD+Met
**
Serum (nmol/L)
liver (nmol/mgprot)
E
Relative mRNA level
NCD
HFD
HFD+Met
**
***
**
Nrf2
Keap1
Ho-1
Nqo1
D
NCD
HFD
HFD+Met
p-Nrf2
Nrf2
β-tubulin
D'
p-Nrf2/Nrf2
*
NCD
HFD
HFD+Met
D''
Nrf2/β-tubulin
*
NCD
HFD
HFD+Met

Figure 3

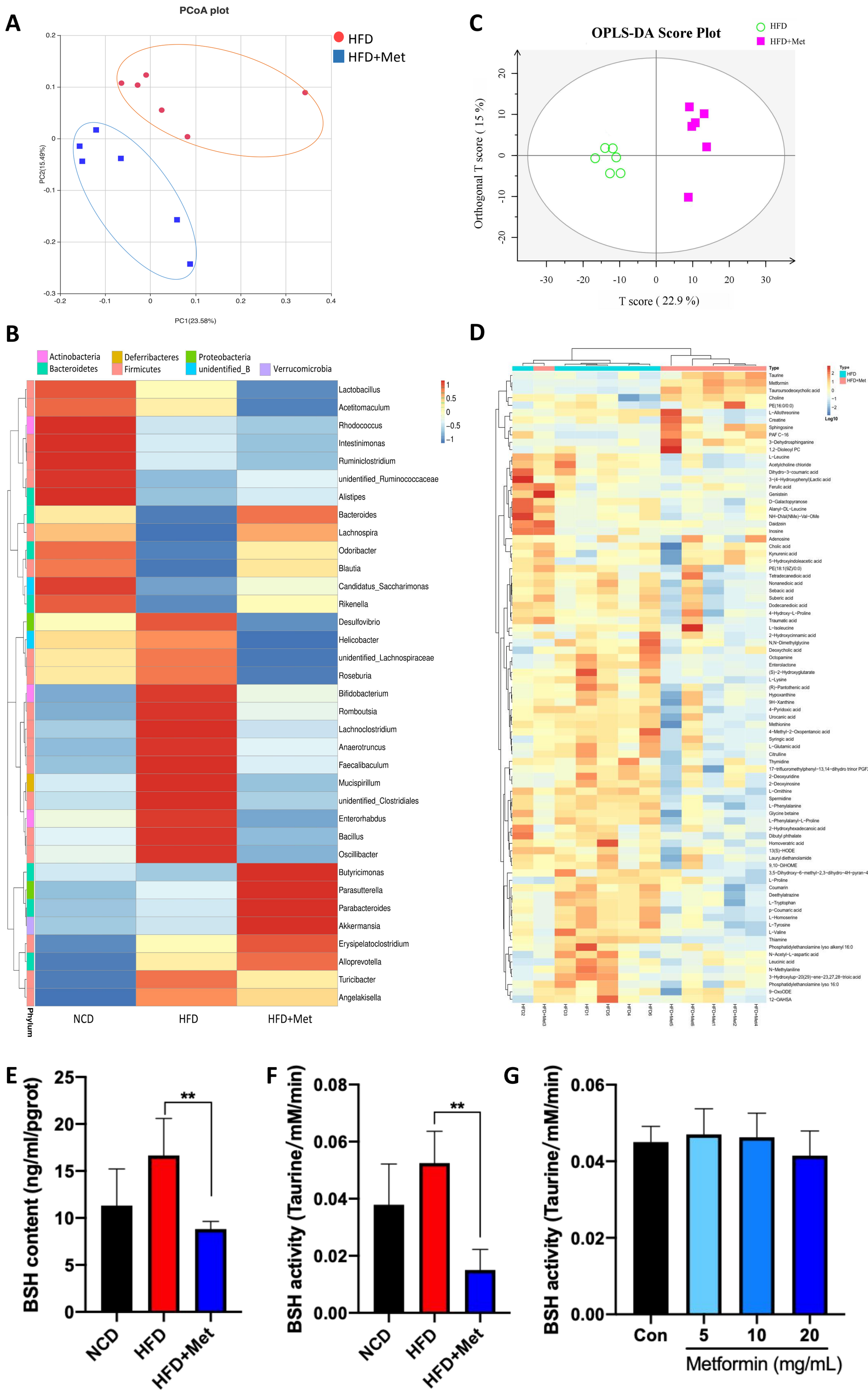
A
PCoA plot
HFD
HFD+Met
PC1(23.58%)
PC2(15.49%)
C
OPLS-DA Score Plot
HFD
HFD+Met
T score (22.9 %)
Orthogonal T score (15 %)
B
Actinobacteria
Bacteroidetes
Deferribacteres
Firmicutes
Proteobacteria
unidentified_B
Verrucomicrobia
Lactobacillus
Acetitomaculum
Rhodococcus
Intestinimonas
Ruminiclostridium
unidentified_Ruminococcaceae
Alistipes
Bacteroides
Lachnospira
Odoribacter
Blautia
Candidatus_Saccharimonas
Rikenella
Desulfovibrio
Helicobacter
unidentified_Lachnospiraceae
Roseburia
Bifidobacterium
Romboutsia
Lachnoclostridium
Anaerotruncus
Faecalibaculum
Mucispirillum
unidentified_Clostridiales
Enterorhabdus
Bacillus
Oscillibacter
Butyricimonas
Parasutterella
Parabacteroides
Akkermansia
Erysipelatoclostridium
Alloprevotella
Turicibacter
Angelakisella
Phylum
NCD
HFD
HFD+Met
D
Type
HFD
HFD+Met
Log10
E
BSH content (ng/ml/pgrot)
NCD
HFD
HFD+Met
F
BSH activity (Taurine/mM/min)
NCD
HFD
HFD+Met
G
BSH activity (Taurine/mM/min)
Con
5
10
20
Metformin (mg/mL)

Figure 4

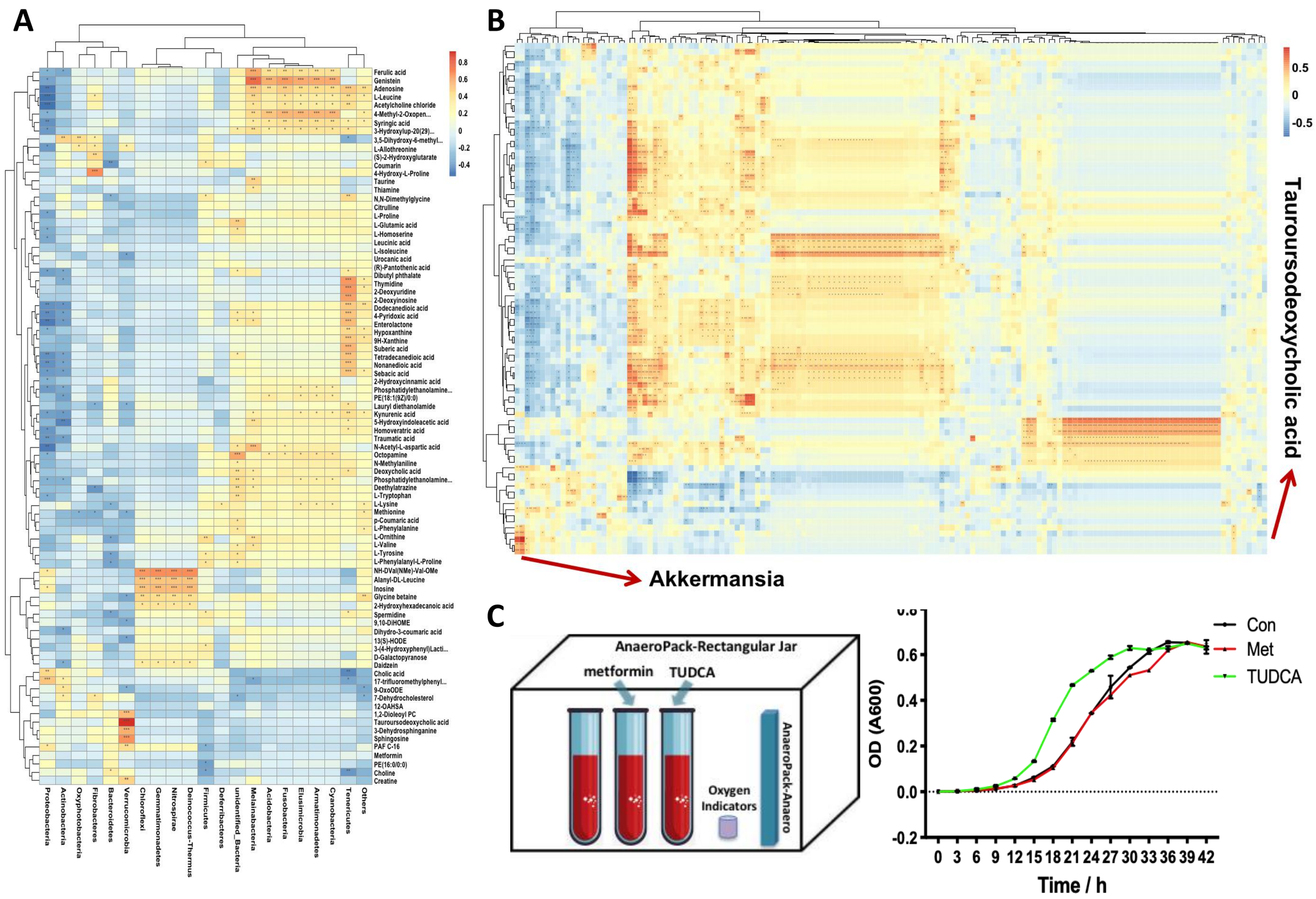
A
B
C
Ferulic acid
Genistein
Adenosine
L-Leucine
Acetylcholine chloride
4-Methyl-2-Oxopen...
Syringic acid
3-Hydroxylup-20(29)...
3,5-Dihydroxy-6-methyl...
L-Allothreonine
(S)-2-Hydroxyglutarate
Coumarin
4-Hydroxy-L-Proline
Taurine
Thiamine
N,N-Dimethylglycine
Citrulline
L-Proline
L-Glutamic acid
L-Homoserine
Leucinic acid
L-Isoleucine
Urocanic acid
(R)-Pantothenic acid
Dibutyl phthalate
Thymidine
2-Deoxyuridine
2-Deoxyinosine
Dodecanedioic acid
4-Pyridoxic acid
Enterolactone
Hypoxanthine
9H-Xanthine
Suberic acid
Tetradecanedioic acid
Nonanedioic acid
Sebacic acid
2-Hydroxycinnamic acid
Phosphatidylethanolamine...
PE(18:1(9Z)/0:0)
Lauryl diethanolamide
Kynurenic acid
5-Hydroxyindoleacetic acid
Homoveratric acid
Traumatic acid
N-Acetyl-L-aspartic acid
Octopamine
N-Methylaniline
Deoxycholic acid
Phosphatidylethanolamine...
Deethylatrazine
L-Tryptophan
L-Lysine
Methionine
p-Coumaric acid
L-Phenylalanine
L-Ornithine
L-Valine
L-Tyrosine
L-Phenylalanyl-L-Proline
NH-DVal(NMe)-Val-OMe
Alanyl-DL-Leucine
Inosine
Glycine betaine
2-Hydroxyhexadecanoic acid
Spermidine
9,10-DiHOME
Dihydro-3-coumaric acid
13(S)-HODE
3-(4-Hydroxyphenyl)Lacti...
D-Galactopyranose
Daidzein
Cholic acid
17-trifluoromethylphenyl...
9-OxoODE
7-Dehydrocholesterol
12-OAHSA
1,2-Dioleoyl PC
Tauroursodeoxycholic acid
3-Dehydrosphinganine
Sphingosine
PAF C-16
Metformin
PE(16:0/0:0)
Choline
Creatine
Proteobacteria
Actinobacteria
Oxyphotobacteria
Fibrobacteres
Bacteroidetes
Verrucomicrobia
Chloroflexi
Gemmatimonadetes
Nitrospirae
Deinococcus-Thermus
Firmicutes
Deferribacteres
unidentified_Bacteria
Melainabacteria
Acidobacteria
Fusobacteria
Elusimicrobia
Armatimonadetes
Cyanobacteria
Tenericutes
Others
0.8
0.6
0.4
0.2
0
-0.2
-0.4
0.5
0
-0.5
Tauroursodeoxycholic acid
Akkermansia
AnaeroPack-Rectangular Jar
metformin
TUDCA
Oxygen Indicators
AnaeroPack-Anaero
OD (A600)
Time / h
Con
Met
TUDCA
0.6
0.4
0.2
0.0
-0.2
0 3 6 9 12 15 18 21 24 27 30 33 36 39 42

Figure 5

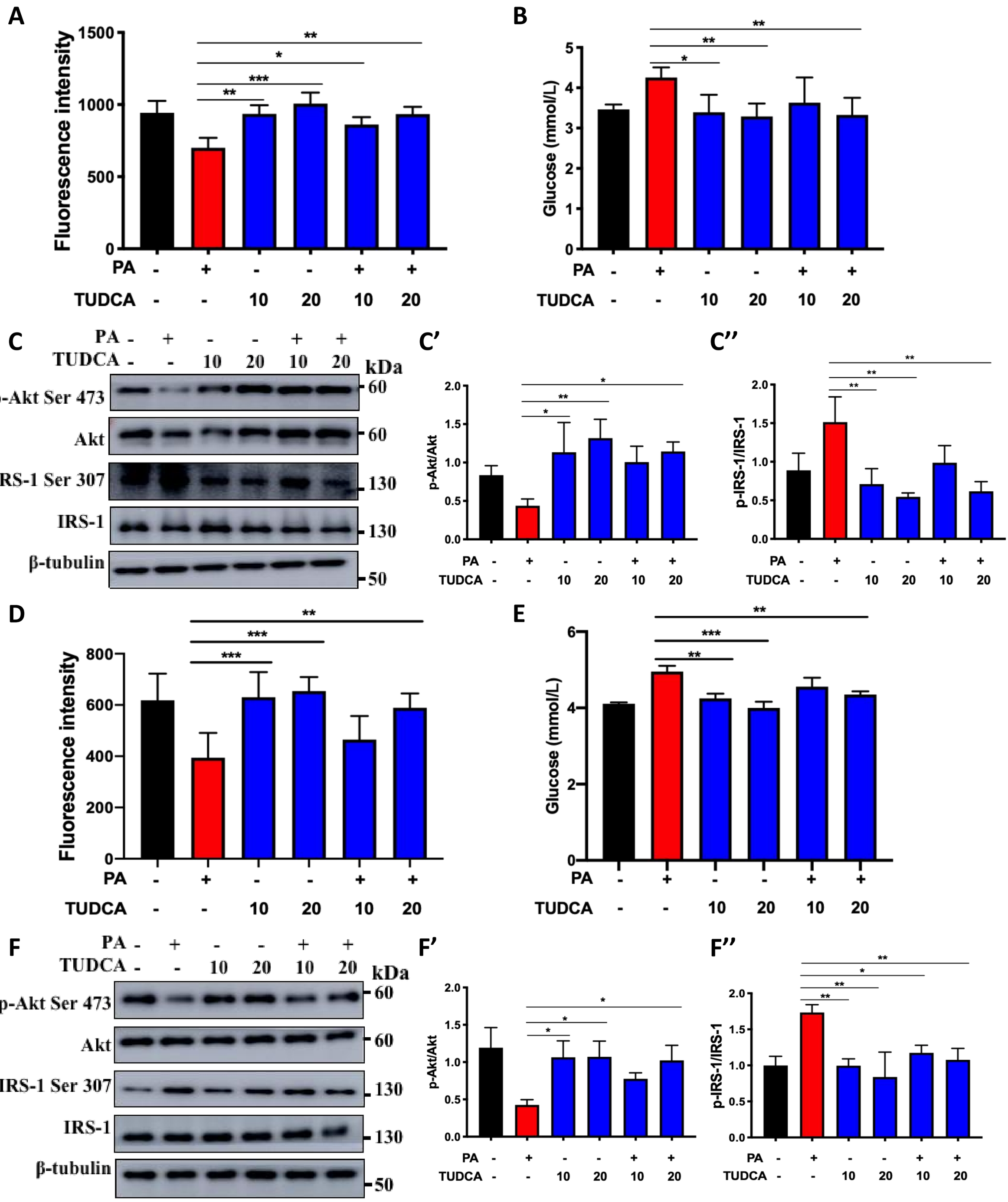
A
Fluorescence intensity
1500
1000
500
0
PA - + - - + +
TUDCA - - 10 20 10 20
B
Glucose (mmol/L)
5
4
3
2
1
0
PA - + - - + +
TUDCA - - 10 20 10 20
C
PA - + - - + +
TUDCA - - 10 20 10 20
kDa
p-Akt Ser 473
Akt
p-IRS-1 Ser 307
IRS-1
β-tubulin
60
60
130
130
50
C'
p-Akt/Akt
2.0
1.5
1.0
0.5
0.0
PA - + - - + +
TUDCA - - 10 20 10 20
C''
p-IRS-1/IRS-1
2.0
1.5
1.0
0.5
0.0
PA - + - - + +
TUDCA - - 10 20 10 20
D
Fluorescence intensity
800
600
400
200
0
PA - + - - + +
TUDCA - - 10 20 10 20
E
Glucose (mmol/L)
6
4
2
0
PA - + - - + +
TUDCA - - 10 20 10 20
F
PA - + - - + +
TUDCA - - 10 20 10 20
kDa
p-Akt Ser 473
Akt
p-IRS-1 Ser 307
IRS-1
β-tubulin
60
60
130
130
50
F'
p-Akt/Akt
2.0
1.5
1.0
0.5
0.0
PA - + - - + +
TUDCA - - 10 20 10 20
F''
p-IRS-1/IRS-1
2.0
1.5
1.0
0.5
0.0
PA - + - - + +
TUDCA - - 10 20 10 20

Figure 6

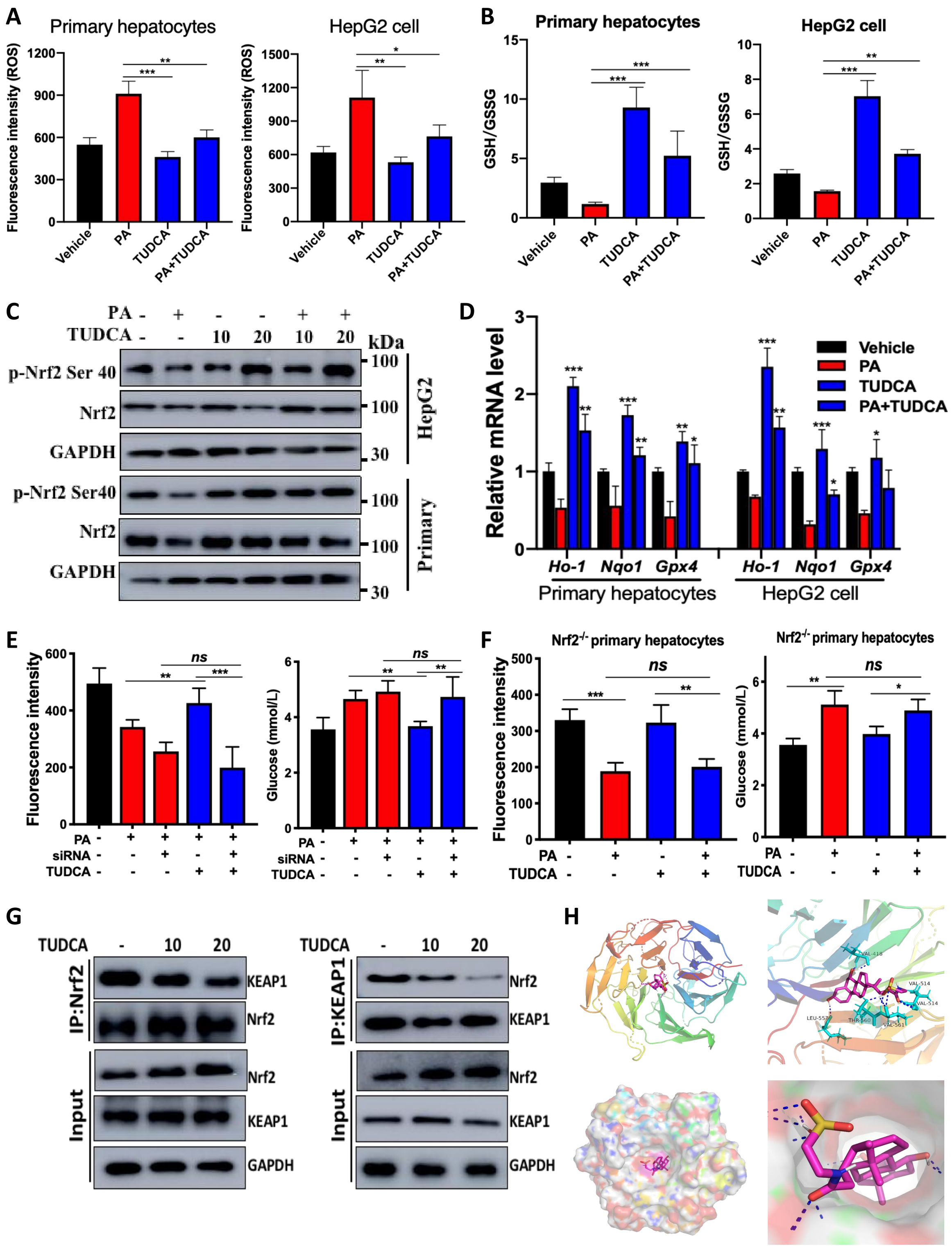
A
Primary hepatocytes
HepG2 cell
Fluorescence intensity (ROS)
Vehicle
PA
TUDCA
PA+TUDCA
B
Primary hepatocytes
HepG2 cell
GSH/GSSG
C
PA
TUDCA
kDa
p-Nrf2 Ser 40
Nrf2
GAPDH
p-Nrf2 Ser40
HepG2
Primary
D
Relative mRNA level
Vehicle
PA
TUDCA
PA+TUDCA
Ho-1
Nqo1
Gpx4
Primary hepatocytes
HepG2 cell
E
Fluorescence intensity
Glucose (mmol/L)
ns
PA
siRNA
TUDCA
F
Nrf2-/- primary hepatocytes
Fluorescence intensity
Glucose (mmol/L)
G
TUDCA
IP:Nrf2
IP:KEAP1
Input
KEAP1
Nrf2
GAPDH
H

Figure 7

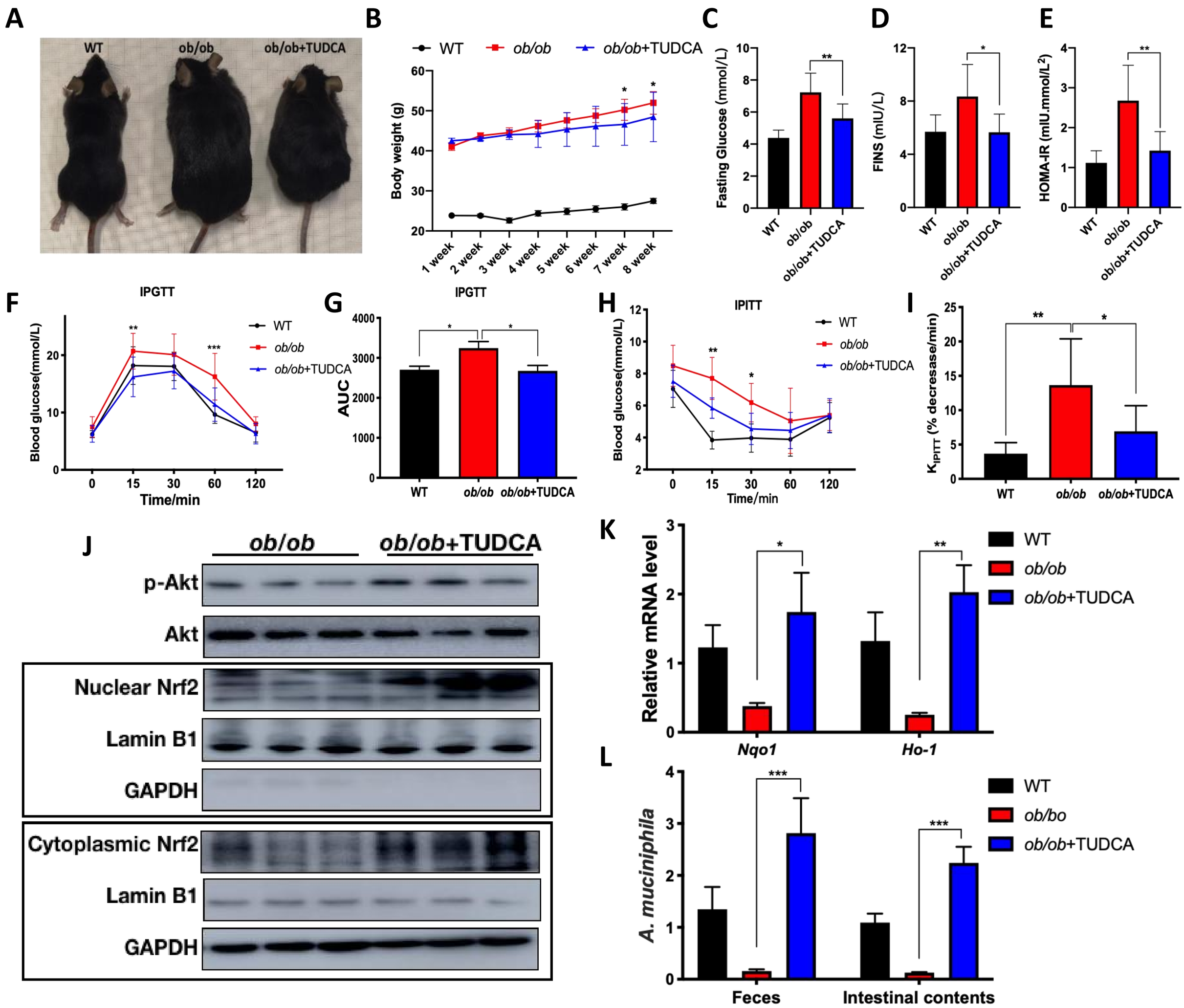
A
WT
ob/ob
ob/ob+TUDCA
B
WT
ob/ob
ob/ob+TUDCA
Body weight (g)
1 week
2 week
3 week
4 week
5 week
6 week
7 week
8 week
C
Fasting Glucose (mmol/L)
D
FINS (mIU/L)
E
HOMA-IR (mIU.mmol/L²)
F
IPGTT
Blood glucose(mmol/L)
Time/min
G
IPGTT
AUC
H
IPITT
Blood glucose(mmol/L)
Time/min
I
K_IPITT (% decresase/min)
J
ob/ob
ob/ob+TUDCA
p-Akt
Akt
Nuclear Nrf2
Lamin B1
GAPDH
Cytoplasmic Nrf2
Lamin B1
GAPDH
K
Relative mRNA level
Nqo1
Ho-1
L
A. muciniphila
Feces
Intestinal contents
ob/bo